

Electronic Thesis and Dissertation Repository

12-17-2020 10:00 AM

The Effect of the Initial Structure on the System Relaxation Time in Langevin Dynamics

Omid Mozafar, *The University of Western Ontario*

Supervisor: Denniston, Colin, *The University of Western Ontario*

A thesis submitted in partial fulfillment of the requirements for the Master of Science degree in Applied Mathematics

© Omid Mozafar 2020

Follow this and additional works at: <https://ir.lib.uwo.ca/etd>



Part of the [Other Applied Mathematics Commons](#)

Recommended Citation

Mozafar, Omid, "The Effect of the Initial Structure on the System Relaxation Time in Langevin Dynamics" (2020). *Electronic Thesis and Dissertation Repository*. 7560.

<https://ir.lib.uwo.ca/etd/7560>

This Dissertation/Thesis is brought to you for free and open access by Scholarship@Western. It has been accepted for inclusion in Electronic Thesis and Dissertation Repository by an authorized administrator of Scholarship@Western. For more information, please contact wlsadmin@uwo.ca.

Abstract

In recent decades, computer experiments have allowed an accurate and fundamental understanding of molecular mechanisms at the microscopic level, such as the process of relaxation at a stable physical state¹. However, computer simulations may sometimes produce non-physical results or relations due to the incompleteness of mathematical models describing physical systems. In this thesis, we have investigated whether the initial structure in a computer simulation affects the system relaxation time, which is denoted by τ_{sys} , in the Langevin $NVT\mathbf{P}$ ² ensemble. We found that for an initial structure, which is inhomogeneous in the number density of atoms, the system relaxation time, τ_{sys} , is longer, often by more than an order of magnitude, compared to that for the homogeneous initial structure. Moreover, we realized that the system relaxation time for the inhomogeneous initial structure is an increasing function of the Langevin coupling constant γ .

Keywords: Relaxation time, The system relaxation time, Inhomogeneous structure, Homogeneous structure, Initial structure, Molecular dynamics simulation, MD, LAMMPS, Computer simulation, Radial distribution function, RDF, Pair distribution function, PDF, Total correlation function, Langevin dynamics, Langevin thermostat, Under-damped Langevin dynamics, Brownian dynamics, Lennard-Jones potential.

¹A stable physical state is a state for which physical properties are finite and time-independent.

² \mathbf{P} is the system's total linear momentum.

Summary for Lay Audience

One of the fundamental physical processes in nature is the relaxation process of many-body systems towards a stable physical state. Once a system equilibrates, it becomes measurable, and thus, we can define reliable physical quantities, such as temperature. That is why conventional physics is mostly defined in steady-state conditions. In this thesis, we are going to measure the time that it takes for a system to reach a steady state under specified conditions using computer simulations. The original objective of doing so is to examine the effects of the initial structural conditions on this period of time, commonly called the system relaxation time and denoted by τ_{sys} . We found that the initial structural conditions have an effect on the system relaxation time. In particular, we have a shorter system relaxation time for homogeneous initial structures than for inhomogeneous initial structures.

Co-Authorship Statement

The work presented in this thesis was done in collaboration with my academic supervisor, Prof. Colin Denniston. Chapter 4 will form the basis for a publication that will also be co-authored with Prof. Denniston.

Acknowledgements

I would first like to thank my thesis supervisor Professor Colin Denniston of the applied mathematics department at Western University. The door to his office was always open whenever I ran into a trouble spot or had any questions concerning my research or writing. He consistently allowed this shared work to be counted as my work, but steered me in the right direction whenever I needed it. I would also like to acknowledge two friends, Mr. Navid Afrasiabian and Ms. Mahtab Amooei, for their generous help in writing this thesis. In the end, I should express my very profound gratitude to my parents, Azar and Ahmad, and my lovely little sister, Setayesh, for providing me with unfailing support as well as continuous encouragement throughout these years of study and research. This accomplishment would not have been possible without them. Thank you all.

Contents

Abstract	ii
Summary for Lay Audience	iii
Co-Authorship Statement	iv
Acknowledgements	v
List of Figures	viii
List of Tables	xi
1 Introduction	1
1.1 The Pair Distribution Function	4
1.2 The Radial Distribution Function	10
1.3 Entropy	12
1.4 Outline	15
2 Theory	17
2.1 Derivation of the Relation between τ_{sys} and $g(r)$	18
3 Methodology	23
3.1 Molecular Dynamics	24
3.1.1 A Brief Review of the GJF and GJF-2GJ Methods	29
3.1.2 Periodic Boundary Conditions	31

3.1.3	Initialization	32
3.1.4	Finite-Size Effects	33
3.1.5	Inter-Particle Interaction Potentials	34
	Lennard-Jones Systems	35
3.1.6	Reduced Units	37
3.2	Simulation Details	38
3.2.1	Measuring the Mean RDF	41
4	Results and Discussion	43
4.1	Temperature Relaxation Time	43
4.1.1	Initial Inhomogeneous Crystalline Structure	43
4.1.2	Initial Homogeneous Crystalline Structure	44
4.2	The Mean RDF	45
4.2.1	Initial Inhomogeneous Crystalline Structure	46
4.2.2	Initial Homogeneous Structure	47
	Crystalline Structure	47
	Amorphous Structure	48
4.3	Discussion	48
4.4	Summary	50
5	Conclusion	52
	Bibliography	54
	Curriculum Vitae	63

List of Figures

1.1	The radial distribution functions of solid at $T = 50K$ (the blue curve), liquid at $T = 80K$ (the black curve), and gaseous Argon at $T = 300K$ (the red curve). The radii are given in the LJ reduced units of the effective atomic radius $\sigma_{Ar} = 3.405\text{\AA}$. From Wikibooks Commons, public domain, URL: https://en.wikibooks.org/w/index.php?title=Molecular_Simulation/Radial_Distribution_Functions&oldid=3710016	6
1.2	Asymptotic behaviour of the function $\ln rh(r)$ for a Lennard-Jones potential, truncated and shifted at $r/\sigma = 2.5$, for $T^* = 1.2$ and two densities $\rho^* = 0.455$ and 0.715 . the asterisk sign * means the quantities are in the LJ reduced units. Adopted from [16] by permission of IOP Publishing with the license ID.: 1075295-1.	7
1.3	Calculation of the radial distribution function $g(r)$. The blue particles have a center that lies within a distance between r and $r + dr$ from the red particle and are counted for the RDF. From Wikipedia Commons, public domain, URL: https://en.wikipedia.org/w/index.php?title=Radial_distribution_function&oldid=978199475	10
3.1	Schematic comparison of the Molecular Dynamics method (in red) and the Monte Carlo method (in blue) sampling the system's potential energy surface. From Wikipedia Commons, public domain, URL: https://en.wikipedia.org/w/index.php?title=Molecular_dynamics&oldid=989719669	25
3.2	Schematic presentation of periodic boundary conditions (PBCs) in 2D. The original simulation box in the middle has eight images around it. From Wikipedia Commons, public domain, URL: https://en.wikipedia.org/w/index.php?title=Periodic_boundary_conditions&oldid=988336659	31

3.3	The reduced Lennard-Jones potential as a function of the reduced distance between a pair of particles. The potential minimum occurs at $r = r_m = 2^{1/6}\sigma$. From Wikipedia Commons, public domain, URL: https://en.wikipedia.org/w/index.php?title=Lennard-Jones_potential&oldid=989336384	36
3.4	Initial crystalline structures (2D representation)	39
3.5	A stabilized amorphous structure (2D representation)	41
4.1	This figure illustrates the evolution of the kinetic temperature T with time during the equilibration phase for an initial inhomogeneous crystalline structure and some multiples of $\gamma = \gamma_0 = 5/7$. As it is evident, the higher the value of the Langevin coupling constant γ , the faster the system reaches thermal equilibrium. The inset depicts that the kinetic temperature relaxation time τ_T varies linearly with $1/\gamma$. To be precise, $\tau_T \simeq 1/2\gamma$. All the values are in the LJ reduced units.	44
4.2	This figure illustrates the time evolution of the kinetic temperature T during the equilibration phase for an initial homogeneous crystalline structure and some multiples of $\gamma = \gamma_0 = 5/7$. As it is obvious, the higher the value of the Langevin coupling constant, the faster the system reaches thermal equilibrium. Besides, the inset shows that the kinetic temperature relaxation time, τ_T , varies with γ as $1/2\gamma$. All the values are in the LJ reduced units.	45
4.3	This figure illustrates $r(g(r) - 1)$ for the case of the inhomogeneous crystalline structure shown in Figure 3.4a, $t_e = 175$, and some multiples of the Langevin coupling constant $\gamma = \gamma_0 = 5/7$. This figure reveals that for an initial heterogeneous structure, the higher the value of the Langevin coupling constant, the more behaviour of the scaled total correlation function deviates from the expected one at thermal equilibrium, i.e., $r(g(r) - 1) = 0$ for $r > r_c (= 2.5)$. The inset shows a zoomed-in version of the figure. All the values are in the LJ reduced units.	46

- 4.4 This figure presents $r(g(r) - 1)$ for the case of the homogeneous crystalline structure of Figure 3.4b, $t_e = 175$, and few multiples of the Langevin coupling constant $\gamma = \gamma_0 = 5/7$. This figure reveals that for an initial homogeneous structure, the scaled total correlation function is independent of γ at thermal equilibrium. The inset shows a zoomed-in version of the figure. All the values are in the LJ reduced units. 47
- 4.5 This figure presents $r(g(r) - 1)$ of the homogeneous crystalline structure of Figure 3.4b for the case of the Langevin coupling constant $\gamma = 2\gamma_0 = 10/7$ and few multiples of $t_e = 175$. This figure demonstrates that the slope of the scaled total correlation function, i.e., $g(r) - 1$, decreases continuously with increasing t_e . The inset shows a zoomed-in version of the figure. All the values are in the LJ reduced units. 49
- 4.6 This figure illustrates how the slope of the scaled total correlation function for $r > r_c (= 2.5)$ changes with the equilibration time t_e . As it is evident, the slope decays exponentially with a γ -dependent time constant, which increases apparently with increasing γ . Based on Equation 2.15, this time constant is the system relaxation time. All the values are in the LJ reduced units. 50
- 5.1 This figure compares the equilibrium and non-equilibrium $\ln r(g(r) - 1)$ for a system which has had an initial inhomogeneous structure in the number density. As $\ln(x)$ of a negative x is not mathematically defined, we plotted $\ln |r(g(r) - 1)|$. All the values are in the LJ reduced units. . . 53

List of Tables

1.1	The thermal average de Broglie wavelength for some different molecular fluids at $T = 50K$. . .	2
3.1	An example of the LJ reduced units for Argon. * The values for ϵ , σ , and m were retrieved from [87].	37
3.2	A series of commands in LAMMPS to create a macroscopically inhomogeneous crystalline structure in number density.	40
3.3	A series of commands in LAMMPS to create a macroscopically homogeneous crystalline structure in number density.	40
3.4	A series of commands in LAMMPS to create a macroscopically homogeneous and stable amorphous structure in the number density of atoms.	41

Chapter 1

Introduction

The liquid state of matter is intuitively perceived as the state that is intermediate between a gas and a solid. The concept of liquid structure (or precisely liquid microstructure) is relatively new in physical chemistry (~ 100 years or more). It has appeared as a convenient way to explain the differences in liquids' properties by differences in their microstructure, just as in other states of matter. It should be noted that how liquid structure is defined plays a crucial role in determining the accuracy of the predicted liquids' properties. In the following paragraphs, we would like to discuss the notion of the liquid structure from the classical statistical mechanics' point of view.

In liquids, atoms and molecules are in a state of permanent thermal motion. This motion is described by classical mechanics (Newtonian or Hamiltonian equations of motion) if the mean nearest-neighbour separation, i.e., $a \equiv \rho^{-1/3}$, where ρ is the number density, is much larger than the thermal average de Broglie wavelength, i.e., Λ , which is a length scale and is defined for a particle of mass m as [1, 2]

$$\Lambda = h/(2\pi mk_B T)^{1/2}, \quad (1.1)$$

where $k_B = 1.381 \times 10^{-23} \text{ JK}^{-1}$ is the Boltzmann's constant, and $h = 6.626 \times 10^{-34} \text{ JS}$ is the Planck's constant. Some examples of the thermal average de Broglie wavelength at temperature $T = 50\text{K}$ are shown in Table 1.1.

In the absence of an unbalanced external influence, the motion is unceasing since particles

Molecule	m^* ($\times 10^{-27}$ Kg)	Λ (\AA)
H_2	3.3471	1.7390
O_2	43.157	0.4365
N_2	46.505	0.4665
F_2	63.095	0.4005

Table 1.1: The thermal average de Broglie wavelength for some different molecular fluids at $T = 50K$.

* Retrieved from the US National Institute of standards and Technology (NIST), public domain, URL: <https://www.nist.gov/pml/atomic-weights-and-isotopic-compositions-relative-atomic-masses>.

move with no friction, and disordered as there is no preferred direction. In classical mechanics, the coupled equations of motion used to describe a many-body system like a liquid are unstable with respect to the initial condition; This is because an infinitesimal error in the determination of initial conditions at $t = 0$ causes an arbitrary large error in the coordinates at all times $t > 0$. The impossibility of determining the particle trajectories is the main property of many-particle systems. Thus, for an extensive collection of particles, we are practically unable to identify the particular point in the phase space ¹ correctly representing the system. This is where statistical mechanics comes into play.

In classical statistical mechanics, many-body systems in the state of chaos² are described by the methods of classical probability theory. For example, for a system consisting of exactly N particles, we introduce an N -particle positional distribution function, $g_N^{(N)}(\mathbf{r}_1, \omega_1, \dots, \mathbf{r}_N, \omega_N; t)$, determining the joint probability of finding the first particle with the orientation ω_1 in the point \mathbf{r}_1, \dots , and the last particle with the orientation ω_N in the point \mathbf{r}_N at time t . The evolution of this function is governed by the BBGKY hierarchy of coupled equations attributed to Bogoliubov, Born, Green, Kirkwood, and Yvon [3–6]. For a system of finitely many particles, although the

¹For mechanical systems, the phase space consists of all possible values of particle positions and momentums.

²Being in the state of chaos means that determining the exact mechanical microstate of the system at each time is practically impossible.

BBGKY hierarchy is a consequence of the so-called N -particle Liouville equation, it contains the N -particle Liouville equation (it is the last equation in the hierarchy) [7]. In thermodynamic equilibrium, $g_N^{(N)}$ becomes proportional to the canonical distribution of Gibbs [7]:

$$g_N^{(N)} \propto \exp\{-U_N/k_B T\}, \quad (1.2)$$

where U_N is the total interaction potential energy.

In equilibrium statistical mechanics, we are interested in the steady-state structure of fluids only. By definition, a steady-state structure must be, on average, time-independent. Hence, in thermodynamic equilibrium, which is a particular class of steady states, the distribution of the relative position of particles is, on average, time-independent. The equilibrium microstructure (or, simply, structure) can thus be defined based on the mean particles' relative positions. It has turned out that defining the equilibrium microstructure in such a way is useful as each state of matter exhibits a special pattern of relative particle positions. The patterns are distinct because they are closely related to structural characteristics. In classical statistical mechanics, the distribution of the relative position of particles is typically described by the two-body distribution function, i.e., $g_N^{(2)}(\mathbf{r}_1, \omega_1, \mathbf{r}_2, \omega_2)$, where [7, 8]

$$g_N^{(2)} \propto \int d\mathbf{r}_3 d\omega_3 \dots d\mathbf{r}_N d\omega_N g_N^{(N)}. \quad (1.3)$$

The two-body distribution function for a translationally-invariant system is conveniently written as $g(\mathbf{r}, \omega_1, \omega_2)$, where $\mathbf{r} = \mathbf{r}_2 - \mathbf{r}_1$, and called the pair distribution function. This function is of great importance in physics as it contains invaluable information on topological symmetries in each state of matter.

In this chapter, we first study the pair distribution function for molecular and atomic fluids. The mathematics supporting each theory is shown and derived wherever it is necessary. Then, in the next two sections, i.e., Sections 1.2 and 1.3, we will focus solely on the radial distribution function and how the equilibrium physical properties could be expressed in terms of it.

1.1 The Pair Distribution Function

In a molecular fluid with an inter-molecular potential $u(\mathbf{r}, \omega_1, \omega_2)$ at equilibrium, the pair distribution function, i.e., $g(12) \equiv g(\mathbf{r}, \omega_1, \omega_2)$, is defined as a quantity proportional to the probability of the presence of a molecule with an orientation of $\omega_2 \equiv \{\phi_2, \theta_2, \chi_2\}$ (Euler angles) at a position of $\mathbf{r} = (r, \theta, \phi)$ relative to a central fixed molecule with a general orientation of $\omega_1 \equiv \{\phi_1, \theta_1, \chi_1\}$ (Euler angles). We should note that the pair distribution function is of fundamental importance to the theory of equilibrium statistical mechanics because almost all of the equilibrium physical properties can be computed once $g(\mathbf{r}, \omega_1, \omega_2)$ is known. Since all the properties of the spherical harmonic functions are so well known and established, it is useful to have a spherical harmonic expansion for $g(\mathbf{r}, \omega_1, \omega_2)$. In a molecular fluid, the harmonic expansion relative to an arbitrary space-fixed reference frame such as the system's center of mass reference frame can generally be written as follows [8–10]:

$$g(\mathbf{r}, \omega_1, \omega_2) = \sum_{l_1 l_2 l} \sum_{m_1 m_2 m} \sum_{n_1 n_2} g(r; l_1, l_2, l; n_1, n_2) C(l_1, l_2, l; m_1, m_2, m) \times D_{m_1 n_1}^{l_1}(\omega_1)^* D_{m_2 n_2}^{l_2}(\omega_2)^* Y_{lm}(\theta, \phi)^*, \quad (1.4)$$

where $g(r; l_1, l_2, l; n_1, n_2)$ are the space-fixed harmonic coefficients, $C(l_1, l_2, l; m_1, m_2, m)$ are the Clebsch-Gordan (CG) coefficients in the convention of Rose (see ref. [11]), $D_{mn}^l(\omega)$ are the generalized spherical harmonics, $Y_{lm}(\theta, \phi)$ are the spherical harmonics, and * indicates a complex conjugate. The $D_{mn}^l(\omega)$ is defined as [12]

$$D_{mn}^l(\omega) \equiv D_{mn}^l(\phi, \theta, \chi) = \exp\{-i(m\phi + n\chi)\} d_{mn}^l(\theta), \quad (1.5)$$

where the function $d_{mn}^l(\theta)$, which represents a rotation of θ about the spherical harmonic Y , can be thought of as a generalized associated Legendre function and written as

$$d_{mn}^l(\theta) \equiv [(l+m)!(l-m)!(l+n)!(l-n)!]^{1/2} \sum_k \frac{(-1)^k (\cos \theta/2)^{2l+m-n-2k} (\sin \theta/2)^{2k-m+n}}{(l+m-k)!(l-n-k)!k!(k-m+n)!}. \quad (1.6)$$

For the case of linear molecules, which are axially symmetric, the coefficients $g(r; l_1, l_2, l; n_1, n_2)$ vanish, unless $n_1 = n_2 = 0$; This is because the pair distribution function should be independent

of the third Euler angle, i.e., χ . For linear molecules, Equation 1.4 reduces then to [8]

$$g(\mathbf{r}, \omega_1, \omega_2) = \sum_{l_1 l_2 l} \sum_{m_1 m_2 m} g(r; l_1, l_2, l) C(l_1, l_2, l; m_1, m_2, m) \times Y_{l_1 m_1}(\omega_1) Y_{l_2 m_2}(\omega_2) Y_{lm}^*(\theta, \phi), \quad (1.7)$$

where

$$g(r; l_1, l_2, l) \equiv \left(\frac{(4\pi)^2}{(2l_1 + 1)(2l_2 + 1)} \right)^{1/2} g(r; l_1, l_2, l; 0, 0). \quad (1.8)$$

For the particular case of monatomic fluids, the coefficients $g(r; l_1, l_2, l)$ vanish, unless $l_1 = l_2 = 0$; This is because atoms do not possess a well-defined orientation and thus, the pair distribution function should be independent of the orientations ω_1 and ω_2 . The pair distribution function of a monatomic (or simply, atomic) fluid can thus be simplified and written as [8]

$$g(\mathbf{r}) = 4\pi \sum_l \sum_m g(r; 0, 0, l; 0, 0) Y_{lm}^*(\theta, \phi). \quad (1.9)$$

For isotropic atomic fluids, the pair distribution function must also be independent of the angles θ and ϕ . As a result, only the coefficient $g(r; 0, 0, 0; 0, 0)$ could be nonzero. The pair distribution function for isotropic atomic fluids can consequently be shown merely as

$$g(\mathbf{r}) = \sqrt{4\pi} g(r; 0, 0, 0; 0, 0). \quad (1.10)$$

The full $g(\mathbf{r}, \omega_1, \omega_2)$ is not yet accessible experimentally, although the projections of g can be measured indirectly. For instance, a series of neutron diffraction experiments on isotropically substituted forms of molecules can yield the so-called centers' pair correlation function, which is denoted by $g(r)$ and mathematically defined as [8]

$$g(r) := \frac{1}{4\pi} \int_0^{2\pi} d\phi \int_0^\pi d\theta \sin \theta \langle g(\mathbf{r}, \omega_1, \omega_2) \rangle_{\omega_1 \omega_2}, \quad (1.11)$$

where $\langle \dots \rangle_{\omega_1 \omega_2}$ is an unweighted average over all the possible molecular orientations and given by

$$\langle \dots \rangle_{\omega_1 \omega_2 \dots \omega_h} \equiv (\Omega_{\omega_1} \Omega_{\omega_2} \dots \Omega_{\omega_h})^{-1} \int \dots d\omega_1 d\omega_2 \dots d\omega_h \quad (1.12)$$

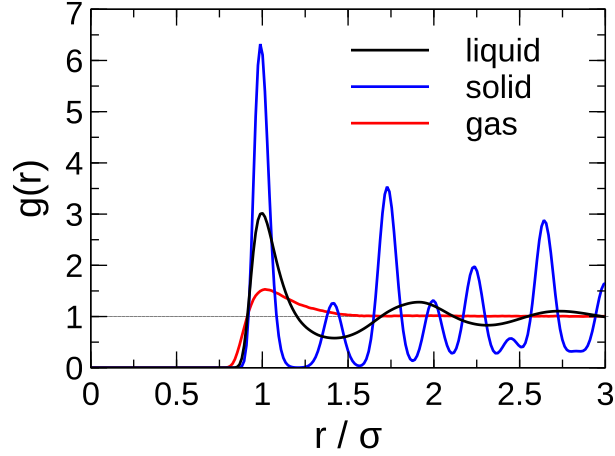


Figure 1.1: The radial distribution functions of solid at $T = 50K$ (the blue curve), liquid at $T = 80K$ (the black curve), and gaseous Argon at $T = 300K$ (the red curve). The radii are given in the LJ reduced units of the effective atomic radius $\sigma_{Ar} = 3.405\text{\AA}$. From Wikibooks Commons, public domain, URL: https://en.wikibooks.org/w/index.php?title=Molecular_Simulation/Radial_Distribution_Functions&oldid=3710016

with

$$\begin{aligned}\Omega_{\omega_i} &= \int d\omega_i = 8\pi^2 \quad \text{for nonlinear molecules} \\ &= 4\pi \quad \text{for linear molecules/atoms.}\end{aligned}\tag{1.13}$$

The centers' pair correlation function, $g(r)$, is a measure of the probability of finding a particle of any shape and orientation at a distance of r from the center of mass of a given reference particle. In the special case of linear molecules/atoms, $g(r)$ is equal to the pair distribution function, given explicitly in Equation 1.10, and is commonly called the radial distribution function. The radial distribution function (or, briefly, RDF) is of particular significance in the physics of fluids. There exist numerous reasons for that; First, $g(r)$ is directly related to the structure factor of the system, denoted by $S(k)$, and can thus be determined experimentally from the radiation scattering experiments such as X-ray diffraction and neutron diffraction [13]. The RDF and the structure factor are related to each other in a uniform fluid via the following expression [14,15]:

$$S(k) = 1 + 4\pi\rho \int_0^\infty dr(g(r) - 1)r^2 \frac{\sin kr}{kr} \quad (\text{for } k \neq 0).\tag{1.14}$$

Second, the form of $g(r)$ provides useful information on the short- and long-range isotropic

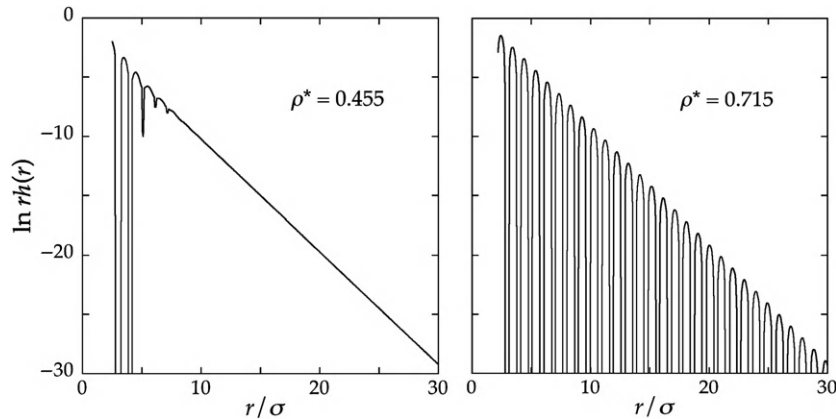


Figure 1.2: Asymptotic behaviour of the function $\ln rh(r)$ for a Lennard-Jones potential, truncated and shifted at $r/\sigma = 2.5$, for $T^* = 1.2$ and two densities $\rho^* = 0.455$ and 0.715 . the asterisk sign * means the quantities are in the LJ reduced units. Adopted from [16] by permission of IOP Publishing with the license ID.: 1075295-1.

structure of fluids and thus, helps us distinguish between different states of matter based on just the topological symmetries [7]. In Figure 1.1, the RDF for different states of matter are shown. As it is evident, the RDF for the solid exhibits a pattern of discrete peaks to indicate the orderly nature of solids. On the contrary, the RDF for fluids has one single distinguished peak at $r \sim \sigma$, so that fluids, unlike solids, only have local orderly structure. The RDF can also be used to link the microscopic structural details to macroscopic properties using the Kirkwood-Buff solution theory [17]. For example, the RDF defines the potential of mean force (PMF) between any pair of particles as [18]

$$PMF(r) \equiv -k_B T \ln g(r). \quad (1.15)$$

For dilute fluids, if the total potential is approximated by a sum of pair potentials $u(r)$, $PMF(r) \simeq u(r)$. The radial distribution function in the limit of zero density can thus be written as

$$\lim_{\rho \rightarrow 0} g(r) = \exp \left\{ -\frac{u(r)}{k_B T} \right\}. \quad (1.16)$$

There is a multitude of papers in the literature attempting to determine the short- and long-range behaviours of the RDF to understand inter-facial phenomena, such as wetting phenomena in liquids [19, 20]. It has rigorously been shown for a fluid at equilibrium with an inter-particle

potential which decays faster than a power law or is truncated at a finite distance, the RDF can, in general, be written as [21–25]

$$rh(r) \equiv r(g(r) - 1) = \sum_n A_n \exp\{ik_n r\}, \quad (1.17)$$

where $h(r)$ is called the total correlation function, and A_n is an amplitude which is proportional to the residue of the Fourier transform of $h(r)$ for the n -th pole, i.e., $k_n = \beta_n + i\alpha_n$ with $\beta_n, \alpha_n \in \mathbb{R}$ and $\alpha_n \geq 0$. It should be noted that the pole or poles with the smallest imaginary part, i.e., α_n , has the slowest exponential rate of decay and dominates the asymptotic behaviour of the scaled total correlation function, i.e., $rh(r)$. Three possible scenarios could happen:

(i) $rh(r)$ decays asymptotically to zero in a pure exponential manner if the leading pole, denoted by k_l and defined as the pole with the smallest α_n , is purely imaginary, namely $k_l^{exp} = i\alpha_l^{exp}$. For such a case, we will have

$$\lim_{r \rightarrow \infty} rh(r) = A_l \exp\{-\alpha_l^{exp} r\} \rightarrow 0. \quad (1.18)$$

(ii) $rh(r)$ decays asymptotically to zero in an exponentially-damped oscillatory manner if there is a conjugate pair of leading poles, instead of one single imaginary pole, namely $k_l^{osc} = \pm\beta_l^{osc} + i\alpha_l^{osc}$ with $\beta_l^{osc} \approx 2\pi/\sigma$, where σ is the effective atomic radius. For such a case, we will have

$$\lim_{r \rightarrow \infty} rh(r) = 2A_l \exp\{-\alpha_l^{osc} r\} \cos \beta_l^{osc} r \rightarrow 0. \quad (1.19)$$

(iii) For real leading poles with $\alpha_l = 0$ and $\beta_l > 0$, $rh(r)$ is purely oscillatory and never decays to zero. Such an asymptotic behaviour is non-physical and corresponds to instability with respect to density modulations in uniform fluids [26, 27]. In a stable equilibrium state, $rh(r)$ decays to zero at $r \rightarrow \infty$.

The cross-over line in the density-temperature plane³ where $\alpha_l^{exp} = \alpha_l^{osc}$ defines the Fisher-Widom line [24]. The curves of the function $\ln(rh(r))$, where $\ln(\dots)$ is the natural logarithm, for two distinct densities in Figure 1.2 illustrate the striking difference in the asymptotic behaviour

³It is a 2D space defined by all the eligible temperatures and densities of a system in thermal equilibrium.

of $g(r)$ at densities on different sides of the Fisher–Widom line for the special case of a truncated and shifted Lennard-Jones potential. The mathematical form of Equations 1.18 and 1.19 makes it natural to identify α_l with the inverse range of $h(r)$, i.e., the inverse correlation length ξ :

$$\xi = (\alpha_l)^{-1}. \quad (1.20)$$

The asymptotic analysis of the RDF is much more complicated for a potential energy which includes power-law contributions. For the common case of the London dispersion forces⁴, the dominant interaction at large r is $u(r) \propto -1/r^6$ (or precisely, $u(r) \propto -1/r^7$ due to screening at intermediate and large distances [30]). In such a case, there will be no imaginary leading poles, and thus, the asymptotic behaviour of $rh(r)$ will only have the following form:

$$\lim_{r \rightarrow \infty} rh(r) = -\frac{C}{r^5} + 2A_l \exp\{-\alpha_l r\} \cos \beta_l r \rightarrow -\frac{C}{r^5} \rightarrow 0, \quad (1.21)$$

where the first term on the right-hand side accounts for the effect of the dispersion forces, and C is some constant proportional to the long-wavelength limit of the structure factor, i.e., $S(0)$. An important point to make is that in the presence of the dispersion forces, one might still define a line similar to the Fisher–Widom line defined above. This line is called a pseudo-Fisher-Widom to emphasize that the actual asymptotic decay of $rh(r)$ is power-law [22].

The so-called pseudo-Fisher-Widom line is defined as a boundary in the density-temperature diagram on which the imaginary part of the pseudo-exponential leading pole, which is defined as the closest pole to the real axis and denoted by $k_l^{pexp} \equiv \beta_l^{pexp} + i\alpha_l^{pexp}$ with $\beta_l^{pexp} \lesssim 0$, is equal to the imaginary part of the high-density pure oscillatory leading poles, i.e., $k_l^{osc} \equiv \pm\beta_l^{osc} + i\alpha_l^{osc}$ with $\beta_l^{osc} \approx 2\pi/\sigma$. On the high-density side of this line, the intermediate-range decay of $rh(r)$ is exponentially-damped oscillatory, and the ultimate long-range decay is proportional to r^{-5} . In contrast, on low-density side of the line, this damped-oscillatory decay is sub-dominant to both

⁴The London dispersion force is a type of temporary attractive force that results when the electron distributions in adjacent atoms fluctuate in time and form temporary dipoles in random directions. This force was named after the German physicist Fritz London [28, 29]

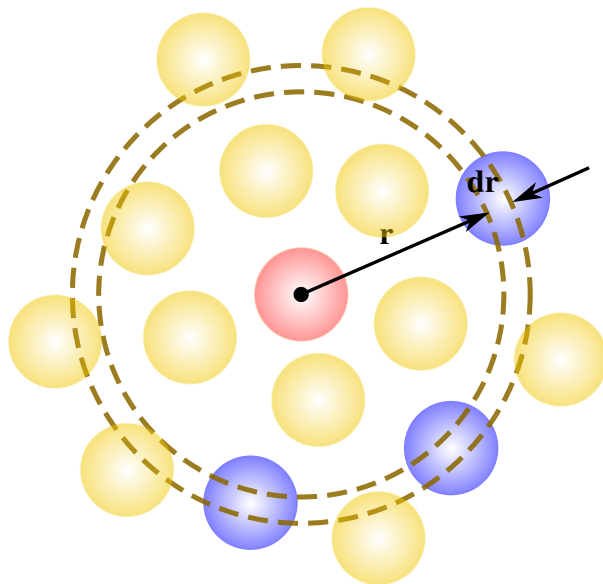


Figure 1.3: Calculation of the radial distribution function $g(r)$. The blue particles have a center that lies within a distance between r and $r + dr$ from the red particle and are counted for the RDF. From Wikipedia Commons, public domain, URL: https://en.wikipedia.org/w/index.php?title=Radial_distribution_function&oldid=978199475

monotonic-exponential and power-law [22]. In the following section, we will focus on the relation of the radial distribution function with the macroscopic structural quantities at equilibrium to see what an important role the RDF plays in understanding fluids.

1.2 The Radial Distribution Function

Let us go back to the definition of the radial distribution function $g(r)$. The radial distribution function represents the probability of finding a (point) particle within a spherical shell of thickness dr at a distance of r from the tagged (point) particle (see Figure 1.3). If the tagged particle (the red particle in Figure 1.3) is taken to be at the origin of coordinates, and if $\rho = N/V$ is the average number density of particles, then the local averaged density at a distance of r from the observer sitting on the tagged particle is simply $\rho g(r)$ [31]:

$$\rho(r) \equiv \rho g(r) = \frac{dn(r)}{dV}, \quad (1.22)$$

where $dn(r)$ is a function which computes the mean number of (point) particles within the shell illustrated in Figure 1.3, and $dV = 4\pi r^2 dr$ is the volume of the shell. The RDF can be evaluated using Equation 1.22 as follows:

$$g(r) = \frac{\rho(r)}{\rho} = \frac{V}{4\pi N r^2} \frac{dn(r)}{dr}, \quad (1.23)$$

where $dn(r)/dr$ represents the rate of change in the number of particles surrounding the central particle at a distance r . In computer simulations, $dn(r)/dr$ can simply be measured. Nevertheless, it is difficult to directly compare structural characteristics found in numerical experiments with natural experiments' results because exactly equivalent methods of measuring geometrical parameters in natural experiments are not available [32]. This is why we need to investigate the relation between the RDF, which represents the structure, and other properties of the system at equilibrium that depend on this structure.

For a uniform, pure atomic fluid, if the total potential energy, U_N , is approximated by a sum of spherically symmetric pair potentials as

$$U_N(\mathbf{r}_1, \mathbf{r}_2, \dots, \mathbf{r}_N) = \frac{1}{2} \sum_{i=1}^N \sum_{j>i}^N u(|\mathbf{r}_j - \mathbf{r}_i|), \quad (1.24)$$

then the mean potential energy per particle, i.e., \mathcal{U} , can be obtained by [33]

$$\mathcal{U} = \frac{1}{2} \int d^3r \rho(r) u(r) = 2\pi\rho \int g(r) u(r) r^2 dr, \quad (1.25)$$

where $\rho(r) = \rho g(r)$ denotes the average density at a distance r from a given particle. The factor $1/2$ has been included to correct for the double-counting of inter-molecular interactions. In the next paragraph, we will study the relation between the pressure and the RDF at equilibrium.

For a uniform atomic fluid under hydrostatic conditions, i.e., at equilibrium, the relationship between the external pressure and internal stress is remarkably simple [34]:

$$P_{ext} = P_{int} = P \quad (1.26)$$

where P_{int} is the internal stress. There are very many different, but equivalent, ways to calculate the pressure of a classical many-body system. The most common one among those is based on

the virial theorem [35]. At equilibrium, the pressure P for pairwise additive interactions can be written as follows:

$$P = P^{id} + \frac{\text{the virial}}{V}, \quad (1.27)$$

where $P^{id} = \rho k_B T$ is the ideal-gas pressure, and the virial is defined as

$$\text{the virial} := -\frac{1}{3} \left\langle \sum_{i=1}^N \sum_{j>i}^N \frac{du(r_{ij})}{dr_{ij}} r_{ij} \right\rangle \equiv -\frac{2\pi}{3} N \rho \int dr r^3 g(r) \frac{du(r)}{dr}. \quad (1.28)$$

By substituting Equation 1.28 back into Equation 1.27, the following expression for the mean pressure P is obtained:

$$P = \rho k_B T - \frac{2}{3} \pi \rho^2 \int r^3 g(r) du(r) \quad (1.29)$$

In the following section, we will discuss the relation between the (mean) entropy and the radial distribution function at some length.

1.3 Entropy

Entropy is a fundamental physical quantity in thermodynamics and statistical mechanics. It was first introduced by Clausius [36] in thermodynamics. Entropy is a function of the macroscopic state of the system. L. Boltzmann in 1872 proposed a microscopic definition for the entropy of an isolated system as follows:

$$S := k_B \ln \Omega(N, N, E) \quad (\text{Boltzmann entropy}), \quad (1.30)$$

where Ω is the number of microscopic states which share the same values of physical quantities of the macroscopic state of the system. Equation 1.30 shows that the more states available to an isolated system, the higher entropy. Later in 1878, J. Willard Gibbs suggested a more general definition for the mean entropy via probabilities of microscopic states of the system as follows:

$$S := -k_B \sum_{i=1}^{\Omega} p_i \ln p_i \quad (\text{Gibbs entropy}), \quad (1.31)$$

where p_i is the probability of the occurrence of the i th microstate with an energy E_i during the system's energy fluctuations. In [37], it was shown that the mean Boltzmann entropy is equal to the Gibbs entropy minus a term indicating the fluctuations of macroscopic physical quantities.

In statistical mechanics, the entropy S of a system at a temperature T with N indistinguishable atoms, described by the canonical coordinates $\mathbf{r}^N = \{\mathbf{r}_1, \mathbf{r}_2, \dots, \mathbf{r}_N\}$ and $\mathbf{p}^N = \{\mathbf{p}_1, \mathbf{p}_2, \dots, \mathbf{p}_N\}$, can be evaluated formally via the generalized Gibbs entropy formula as follows [38, 39]:

$$S(N, V, T) = -\frac{k_B}{N!} \int_V d\mathbf{r}^N \int_{-\infty}^{\infty} d\mathbf{p}^N f_c(\mathbf{r}^N, \mathbf{p}^N) \ln [h^{3N} f_c(\mathbf{r}^N, \mathbf{p}^N)] \quad (1.32)$$

in the canonical ensemble. In this expression, the factor of $1/N!$ corrects for the redundancy of configurations of identical particles, and the factors of Planck's constant h are derived from the quantum mechanical expression. Also, $f_c(\mathbf{r}^N, \mathbf{p}^N)$ is the canonical ensemble probability density that the phase point $(\mathbf{r}^N, \mathbf{p}^N)$ is occupied, and is given by

$$f_c(\mathbf{r}^N, \mathbf{p}^N) = N! \frac{\exp\{-H(\mathbf{r}^N, \mathbf{p}^N)/k_B T\}}{\int_V d\mathbf{r}^N \int_{-\infty}^{\infty} d\mathbf{p}^N \exp\{-H(\mathbf{r}^N, \mathbf{p}^N)\}}, \quad (1.33)$$

whose normalization is

$$N! = \int_V d\mathbf{r}^N \int_{-\infty}^{\infty} d\mathbf{p}^N f_c(\mathbf{r}^N, \mathbf{p}^N). \quad (1.34)$$

If the Hamiltonian H separates into additive terms for the configurational and kinetic energies, the probability density can be factorized into a product as follows:

$$f_c(\mathbf{r}^N, \mathbf{p}^N) = g_N^{(N)}(\mathbf{r}^N) \prod_{i=1}^N f_N^{(1)}(\mathbf{p}_i), \quad (1.35)$$

where $f_N^{(1)}(\mathbf{p}_i)$ is called the one-particle probability density and defined as

$$f_N^{(1)}(\mathbf{p}_i) = \rho(2\pi m k_B T)^{-3/2} \exp\{-|\mathbf{p}_i|^2/2m k_B T\}. \quad (1.36)$$

Equation 1.35 serves as a definition for the N -particle positional distribution function, $g_N^{(N)}(\mathbf{r}^N)$, introduced earlier in the Introduction; $g_N^{(N)}(\mathbf{r}_1, \dots, \mathbf{r}_N)$ is the joint probability of finding particle 1 at position \mathbf{r}_1 , ..., and particle N at position \mathbf{r}_N . Let us next introduce a factorization of the N -particle positional distribution in a certain way using the Generalized Kirkwood Superposition

Approximation (GKSA) as follows [40, 41]:

$$\begin{aligned}
g_N^{(N)}(\mathbf{r}_1, \dots, \mathbf{r}_N) &= g_N^{(2)}(\mathbf{r}_1, \mathbf{r}_2) \times \dots \times g_N^{(2)}(\mathbf{r}_{N-1}, \mathbf{r}_N) \\
&\times \delta g_N^{(3)}(\mathbf{r}_1, \mathbf{r}_2, \mathbf{r}_3) \times \dots \times \delta g_N^{(3)}(\mathbf{r}_{N-2}, \mathbf{r}_{N-1}, \mathbf{r}_N) \\
&\times \dots \times \delta g_N^{(N)}(\mathbf{r}_1, \dots, \mathbf{r}_N),
\end{aligned} \tag{1.37}$$

where

$$\delta g_N^{(3)}(\mathbf{r}_1, \mathbf{r}_2, \mathbf{r}_3) \equiv \frac{g_N^{(3)}(\mathbf{r}_1, \mathbf{r}_2, \mathbf{r}_3)}{g_N^{(2)}(\mathbf{r}_1, \mathbf{r}_2)g_N^{(2)}(\mathbf{r}_1, \mathbf{r}_3)g_N^{(2)}(\mathbf{r}_2, \mathbf{r}_3)}, \tag{1.38}$$

$$\delta g_N^{(4)}(\mathbf{r}_1, \mathbf{r}_2, \mathbf{r}_3, \mathbf{r}_4) \equiv \frac{g_N^{(4)}(\mathbf{r}_1, \mathbf{r}_2, \mathbf{r}_3, \mathbf{r}_4)}{g_N^{(2)}(\mathbf{r}_1, \mathbf{r}_2) \dots g_N^{(2)}(\mathbf{r}_2, \mathbf{r}_3) \delta g_N^{(3)}(\mathbf{r}_1, \mathbf{r}_3, \mathbf{r}_4) \dots \delta g_N^{(3)}(\mathbf{r}_2, \mathbf{r}_3, \mathbf{r}_4)}, \tag{1.39}$$

and so forth. By substituting Equation 1.35 back into Equation 1.32 and using Equations 1.36 and 1.37, we find an expansion for the entropy $s \equiv S/N$ which is expected to be well-convergent at high and low densities [42–44]:

$$s = \sum_n s_n = s_1 + s_2 + \dots, \tag{1.40}$$

where s_n is called the n-body entropy,

$$s_1 = k_B \left[\frac{3}{2} - \ln \rho \Lambda^3 \right] \tag{1.41}$$

with $\Lambda = h/(2\pi m k_B T)^{1/2}$ being the thermal average de Broglie wavelength, and

$$s_2 = k_B \left[-2\pi\rho \int [g(r) \ln g(r)] r^2 dr \right] = \frac{2\pi\rho}{T} \int g(r) PMF(r) r^2 dr, \tag{1.42}$$

with $PMF(r)$ being the potential of mean force between any two particles. We can separate the $PMF(r)$ approximately into two additive terms for a dilute system whose total potential energy is given by a sum of independent pair potentials:

$$PMF(r) = u(r) + \delta u(r), \tag{1.43}$$

where $u(r)$ is the pair potential, and $\delta u(r)$ is the energy contribution because of the presence of other particles in the system. Strictly speaking, $\delta u(r)$ indicates the change in the free Helmholtz

energy of the solvent caused by moving any two particles i and j from $|\mathbf{r}_j - \mathbf{r}_i| = \infty$ to $|\mathbf{r}_j - \mathbf{r}_i| = r$. Clearly, in the limit of zero number density, we should have [18]

$$\lim_{\rho \rightarrow 0} \delta u(r) = 0 \quad (1.44)$$

for a uniform system in thermodynamic equilibrium⁵. By replacing PMF in Equation 1.42 with the expression given in Equation 1.43, the following expression for dilute systems is obtained:

$$s_2 = \frac{2\pi\rho}{T} \int g(r)u(r)r^2 dr + \frac{2\pi\rho}{T} \int g(r)\delta u(r)r^2 dr = \frac{\mathcal{U}}{T} + \delta s_2, \quad (1.45)$$

where \mathcal{U} is the mean potential per particle, and δs_2 is the entropy contribution due to surrounding particles. Strictly speaking, δs_2 is associated with the intermediate and long-range order in a system. Hence, it should be zero for a system in which the intermediate and long-range order is absent.

For dilute systems, the entropy s can approximately be written as

$$s = s_1 + s_2 + \frac{k_B}{2} \quad (\text{for dilute systems}), \quad (1.46)$$

where the third term on the right-hand side, i.e., $k_B/2$, is the approximate contribution of higher-order terms to the entropy s [45]. Studies of this approximation, for the Lennard-Jones systems by Baranyai and Evans [45] and the hard-sphere systems by Mountain and Raveché [46], have shown that this approximation is also valid for a dense system whose mass density is near the freezing point. It has been proven that this apparent agreement at high densities is principally because of a fortuitous cancellation of relatively large, higher-order terms [47].

1.4 Outline

In this thesis, we are going to investigate the effect of initial structure on the relaxation time of a computer-simulated system, where the time-averaged kinetic energy per particle is maintained

⁵A system is said to be in thermodynamic equilibrium if there exists no net change in its macroscopic properties with time. Strictly speaking, thermodynamic equilibrium is a combination of thermal, mechanical, chemical, and radioactive equilibria.

by the Langevin thermostat⁶. In the next chapter, we will derive an original expression which connects the system relaxation time, τ_{sys} , to the RDF. This expression is the cornerstone of this thesis as we use it to interpret the results. In chapter 3, we will provide the details on simulation methods and system features. Then, in chapter 4, we will present the results obtained from our computer simulations. Finally, we summarize the thesis with some conclusions and suggestions in chapter 5.

⁶Langevin thermostat is a local stochastic thermostat and maintains the temperature through a modification of Newton's equations of motion named Langevin equation. The Langevin equation was named after Paul Langevin and is a stochastic differential equation describing the time evolution of the system [48].

Chapter 2

Theory

In statistical mechanics, one can show that any non-equilibrium distribution decays eventually (not necessarily monotonically) to a steady-state distribution¹. Moreover, under general conditions, any deviation from a steady-state distribution breaks the temporal translational symmetry (TTS)² in the system. As indicated, the characteristic time of the process which determines how fast the system retrieves the time translational symmetry is called the system relaxation time³ and denoted by τ_{sys} . In this chapter, we will derive an original expression relating the system relaxation time to $g(r)$ to determine the effects of the initial structure on the system relaxation by examining the behaviour of the RDF during the system's equilibration. For this purpose, we need first to study the Helmholtz free energy since its equilibration is equivalent to the system's equilibration for a closed NVT system⁴.

¹Not necessarily to an equilibrium steady-state distribution.

²Temporal translational symmetry (TTS) states that the laws of physics are the same throughout history. In other words, we can move the origin of time coordinate without violating any conservation law. The interested reader is referred to Ref. [49] to read about the new and astonishing discovery of time crystals.

³The word “relaxation” was first used by James Clerk Maxwell in his paper named “On the Dynamical Theory of Gases” in 1867 [50].

⁴A closed NVT system refers to a system which has a constant total number of particles N , total volume V , and is in thermal contact with a heat bath at temperature T .

2.1 Derivation of the Relation between τ_{sys} and $g(r)$

The Helmholtz free energy for a closed NVT system is defined as [51]

$$F := E - TS, \quad (2.1)$$

where $E = 3/2Nk_B T + N\mathcal{U}$ is the time-averaged total energy of a monatomic fluid, $S = Ns = N(s_1 + s_2 + \dots)$ is the mean entropy of the system, and T is the absolute equilibrium temperature of surroundings, modelled as a thermal bath. The Helmholtz free energy F is a thermodynamic potential which determines the “useful” work retrievable from a closed NVT system. In other words, the negative of the difference in the Helmholtz energy is equal to the maximum amount of work extractable from a thermodynamic process in which both temperature T and volume V are kept constant. Under these conditions, F is minimized and held constant at thermodynamic equilibrium [52]. Helmholtz free energy F has the dimensions of energy and is a state quantity; namely, its value is determined by the physical state, not by its history.

Let us interpret the Helmholtz free energy F more concretely as follows:

Imagine creating a system with a mean net entropy S and a mean total energy E in contact with an environment at temperature T . How much energy must be provided? Some of the energy E can be obtained as heat from the environment – this heat is TS , where S is the mean entropy of the created system. The rest of the energy E must be provided somehow as mechanical work – this work is F [53].

By replacing E and S with their equivalent expressions in Equation 2.1 and also, by using Equations 1.41, 1.45, and 1.46, we can write the low-density limit of the Helmholtz free energy per particle, i.e., $f \equiv F/N$, for an isotropic and homogeneous monatomic closed system with a short-range potential energy as

$$f = k_B T \left[\ln \rho \Lambda^3 - \frac{1}{2} \right] - T \delta s_2 = f^{id}(T) + f^{exc}(\delta s_2) \quad (\text{for dilute systems}), \quad (2.2)$$

where $f^{id} = k_B T \left[\ln \rho \Lambda^3 - \frac{1}{2} \right]$ is the ideal-gas Helmholtz free energy per particle, and f^{exc} is the

excess Helmholtz free energy per particle with this feature

$$\lim_{\rho \rightarrow 0} f^{exc} = - \lim_{\rho \rightarrow 0} T \delta s_2 = 0 \quad (2.3)$$

for a uniform closed NVT system in thermodynamic equilibrium. Before studying the system relaxation time, denoted by τ_{sys} , we should introduce a particular kind of mathematical systems called exponentially ergodic systems.

The exponentially ergodic system is a mathematical system for which any dynamical quantity, say A , is expected to relax thermally from its initial equilibrium value A^i at the temperature T^i to the equilibrium value A^f at the temperature $T^f (\neq T^i)$ according to the following approximate formula [54]:

$$\langle A(t) \rangle = A^f + (A^i - A^f) \exp\{-t/\tau_A\}, \quad (2.4)$$

where $\tau_A > 0$ is the characteristic relaxation time for the quantity $A(t)$ and is defined as the time required for $A(t)$ to come to equilibrium with its surrounding medium. The temperature switch occurs at time $t = 0$, and the angle brackets denote an average over an ensemble of independent experiments. The subscript on τ_A indicates that different dynamical quantities might equilibrate with different rates. Thus, the system's relaxation rate should be estimated from the maximum value of τ_A in a system, i.e.,

$$\tau_{sys} = \tau_A^{max}. \quad (2.5)$$

For the canonical ensemble, the system relaxation time, τ_{sys} , is equal to the relaxation time for the Helmholtz free energy, F (or equivalently, $f \equiv F/N$). Based on Equation 2.2, once the temperature T and δs_2 equilibrate, so will f . Hence, we could write the system relaxation time for this limiting case, i.e., dilute systems, as follows:

$$\tau_{sys} = \tau_f = MAX\{\tau_T, \tau_r\}, \quad (2.6)$$

where τ_T and τ_r are the relaxation times for temperature T and residual entropy δs_2 , respectively. Equation 2.6 also implies that τ_{sys} does not depend on the relaxation time of the mean

potential energy, i.e., τ_u . Hence, in a closed NVT system, the equilibration of the mean potential energy is not necessarily equivalent to the equilibration of the system. This point has been overlooked in some previous works, such as [54]. In equilibrium statistical mechanics, temperature can be defined via the equipartition theorem [55] as the time-averaged kinetic energy of each particle. So, it is a local quantity and should generally equilibrate faster than the residual entropy, whose equilibration depends on the equilibration of the position of so many particles. In other words, we always have $\tau_r \geq \tau_T$ and as a consequence,

$$\tau_{\text{sys}} = \tau_r. \quad (2.7)$$

In the next paragraph, we would like to investigate the relation between τ_r and $g(r)$ as the RDF can be measured directly in a computer experiment.

In an exponentially ergodic system, it is not always possible to approximate the evolution of dynamical quantities to equilibrium with Equation 2.4, especially when the system undergoes a first-order phase transition. For example, entropy changes abruptly during a first-order phase transition. However, we expect that the effects of a first-order transition on dynamical quantities vanish long after the equilibration of temperature T . Therefore, the evolution of $T\delta s_2$ in a dilute system during a spontaneous structural process⁵, following Equation 1.45, could be written for $t \gg \tau_T$ as

$$\begin{aligned} \langle T\delta s_2(t) \rangle &= 2\pi\rho \int \langle g(r, t)\delta u(r, t) \rangle r^2 dr \\ &= 2\pi\rho \int \langle \exp\{-PMF(r, t)/k_B T\}\delta u(r, t) \rangle r^2 dr, \end{aligned} \quad (2.8)$$

where $g(r, t) \equiv \exp\{-PMF(r, t)/k_B T\}$ is called instantaneous RDF and the same as the so-called van Hove distribution function, denoted by $G(r, t)$ [56]. This equation can be further simplified by using the generalized version of Equation 1.43⁶:

$$\langle T\delta s_2(t) \rangle = 2\pi\rho \int \exp\{-u(r)/k_B T\}\langle \exp\{-\delta u(r, t)/k_B T\}\delta u(r, t) \rangle r^2 dr. \quad (2.9)$$

⁵In thermodynamics, a spontaneous process is a self-driven irreversible process towards an equilibrium state that minimizes the system's Helmholtz free energy F .

⁶Note that Equation 1.43 is time-independent. However, one could generalize it for dilute systems to include

By expanding $\exp\{-\delta u(r, t)/k_B T\}$ into a power series in $u(r, t)$ and also, approximating $\langle \delta u(r, t) \rangle$ with $\Delta u(r) \exp\{-t/\tau_{\delta u}\}$ for an exponentially ergodic system, where $\Delta u(r) \equiv \delta u(r, t_m) - \delta u(r, t_f)$ is called residual potential energy with $t_m \gg \tau_T$ being an intermediate time during the system's equilibration and t_f as the final time, we find the following series for $t \gg \tau_T$:

$$\langle T \delta s_2(t) \rangle = \sum_{n=0}^{\infty} T \delta s_2^n \exp\{-t/\tau_{\delta u}^n\}, \quad (2.10)$$

where δs_2^n is the n th-moment of the residual two-body entropy and is defined as

$$\delta s_2^n \equiv \frac{2\pi\rho}{T} \int e^{-u(r)/k_B T} \frac{(-1)^n \Delta u(r)^{n+1}}{n!(k_B T)^n} r^2 dr, \quad (2.11)$$

and the corresponding relaxation time is given by

$$\tau_{\delta u}^n \equiv \frac{\tau_{\delta u}}{n+1} \quad \text{for } n = 0, 1, \dots, \quad (2.12)$$

which is a maximum for $n = 0$. Hence, $\tau_{\delta u}$, the relaxation time of the residual potential energy, is equal to τ_r since, by definition, $\tau_r = \text{MAX}\{\tau_{\delta u}^n\}$.

In the low-density limit, we can write the RDF during the system's equilibration as follows for $\tau_T \ll t < \tau_r$:

$$\begin{aligned} \langle g(r, t) \rangle &= \langle \exp\{-PMF(r, t)/k_B T\} \rangle = \exp\{-u(r)/k_B T\} \langle \exp\{-\delta u(r, t)/k_B T\} \rangle \\ &= \exp\{-u(r)/k_B T\} \left(\sum_{n=0}^{\infty} \frac{(-1)^n \langle \delta u(r, t) \rangle^n}{n!(k_B T)^n} \right), \end{aligned} \quad (2.13)$$

where the Taylor series expansion in the parentheses can be approximated by the first two terms as $\langle \delta u(r, t) \rangle \approx 0$ for dilute systems. If the pair potential $u(r)$ is considered short-range, then for $r \gg r_c$, where r_c is the effective range of the pair potential, we could write the total correlation function, $h \equiv g - 1$, as

$$\langle h(r, t) \rangle \equiv \langle g(r, t) \rangle - 1 = -\frac{\langle \delta u(r, t) \rangle}{k_B T}. \quad (2.14)$$

time as well. The simplest generalization can be written as follows:

$$PMF(r, t) = u(r) + \delta u(r, t),$$

where $\delta u(r, t)$ is the correction to the pair potential at time t due to the mean-field effect of surrounding particles during the system's equilibration.

If we replace $\langle \delta u(r, t) \rangle$ again with the expression $\Delta u(r) \exp\{-t/\tau_{\delta u}\}$ for an exponentially ergodic system and employ the fact that $\tau_{\delta u} = \tau_r$ (and $\tau_r = \tau_{sys}$), we will attain the following expression for $r \gg r_c$ and $\tau_T \ll t < \tau_{sys}$:

$$\langle h(r, t) \rangle = -\frac{\Delta u(r)}{k_B T} \exp\{-t/\tau_{sys}\} \quad (\text{for dilute systems}). \quad (2.15)$$

Equation 2.15 is of great importance as it relates the equilibration of the total correlation function $h(r) \equiv g(r) - 1$ to both the residual potential energy, $\Delta u(r)$, and the system relaxation time, τ_{sys} , in dilute systems. If a system's initial structure is more compacted than the final structure, $\Delta u(r) = \delta u(r, t_m) - \delta u(r, t_f) < 0$. As a result, from Equation 2.15, h approaches its equilibrium value at large distances r , i.e., zero, from positive values. On the other hand, if the initial structure is more expanded than the final structure, h approaches zero from negative values because $\Delta u(r) = \delta u(r, t_m) - \delta u(r, t_f) > 0$. Equation 2.15 is one the primary results of this thesis.

Chapter 3

Methodology

The radial distribution function $g(r)$ is an observable that characterizes the time-averaged structure of different states of matter. As a consequence, it is of great significance in physics. In the previous chapters, we showed how the RDF could be related to thermodynamic quantities, such as the mean pressure P and entropy S . Furthermore, we showed that the RDF equilibrates with the same rate as a dilute system does. The only drawback of the radial distribution function is that it is difficult to measure it directly in a natural experiment¹. However, the invention of new methods of conducting experiments with the advancement of computers solves this drawback of $g(r)$. Arguably, the best-known methods are that of “Monte Carlo” and “Molecular Dynamics” simulations. Both of these methods aim to provide information about physical properties of samples.

The Monte Carlo simulation method is a computer simulation experimental method, which uses random numbers to provide a stochastic model for physical phenomena. Metropolis and Ulam coined the name “Monte Carlo” (see, for example, Ref. [57]). A Monte Carlo simulation generates an ensemble of representative configurations under specific thermodynamics conditions for a many-particle system [58]. Monte Carlo simulations do not provide any information on the evolution of systems in time. Instead, they provide an ensemble of independent configura-

¹A natural experiment is one done in a real laboratory with real substances and equipment.

rations and consequently, conformations from which probabilities and relevant thermodynamic observables such as the free Helmholtz energy may be calculated [59].

The Molecular Dynamics method is a deterministic computer experimental method, which is a powerful tool in studying the temporal and spatial evolution of a system's properties. By studying the numerical integration algorithms in Molecular Dynamics simulations, we not only can analyze the local and global structure, the motion of particles, and the image of the macroscopic relation between them and the substance, but can also investigate the relation between the interaction and the macroscopic properties much more conveniently than in the Monte Carlo method. In this method, the particle trajectories are typically determined by numerically solving Newton's equations of motion. Alder and Wainwright reported the first proper Molecular Dynamics simulations in 1956 at Livermore, California, focusing on the hard-sphere systems' dynamics (see Ref. [60]).

Unlike the Molecular Dynamics (MD) method, the Monte Carlo (MC) method is of stochastic nature. This means that with the same initial conditions, the MD method will always generate identical trajectories in the phase space, but not the MC method. Another significant difference between these two simulating methods is that physical quantities are sampled sequentially over time in the Molecular Dynamics simulations. However, in Monte Carlo simulations, the sampling does not follow the direction of time, and as a consequence, none of the data is temporally related (see Figure 3.1). Since we are interested only in how a system equilibrates here, we will use Molecular Dynamics simulations in this thesis.

3.1 Molecular Dynamics

The idea behind Molecular Dynamics is relatively simple:

A number of fictitious particles representing molecules/atoms with initial positions and velocities and interacting via certain interaction potentials are created. Then, the computer calculates the net force on every particle. Let particle i be subject to a net force \mathbf{F}_i at instant t . Molecular

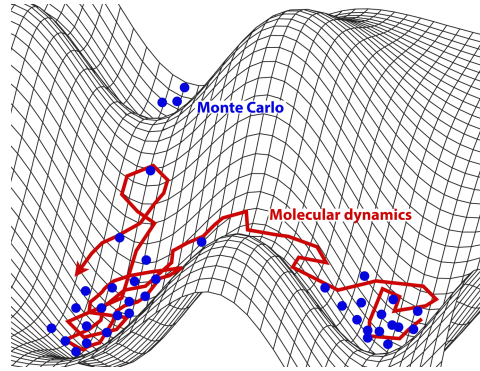


Figure 3.1: Schematic comparison of the Molecular Dynamics method (in red) and the Monte Carlo method (in blue) sampling the system's potential energy surface. From Wikipedia Commons, public domain, URL: https://en.wikipedia.org/w/index.php?title=Molecular_dynamics&oldid=989719669.

Dynamics should then solve the following coupled equations of motion:

$$m_i \frac{d^2 \mathbf{r}_i}{dt^2} = \mathbf{F}_i(\mathbf{r}_1, \mathbf{r}_2, \dots, \mathbf{v}_1, \mathbf{v}_2, \dots) \quad \text{for } i = 1, 2, \dots, \quad (3.1)$$

where the force generally depends on the position and velocity of all particles, to calculate new velocities and positions. A computer solves the coupled equations numerically, so that time is broken down into small time steps Δt . Every time step, the forces are calculated, and positions are updated. These discrete time steps will cause a severe issue as the events that happen over a time step are ignored. This severe issue, which is usually referred to as the discretization error, can be reduced by reducing the timestep size or using a more accurate algorithm for integrating the forces. Following [61], we can expect that for a system whose potential energy is bounded from below, the resulting equilibrium distribution is different from the true theoretical one, as shown below [62]:

$$P_{sim} = P_{true} \sum_{n=1}^{\infty} \exp\{\Delta t^n C_n / k_B T\}, \quad (3.2)$$

where is P_{sim} the equilibrium distribution generated in computer simulations, P_{true} is the true theoretical equilibrium distribution, and C_n is some algorithm-dependent coefficient. The first nonzero C_n yields the correction to the true equilibrium distribution generated by the numerical scheme. To avoid the discretization error, the MD time step Δt , for instance, should be smaller

than the fastest vibrational frequency of the system.

Overall, a typical Molecular Dynamics program follows this scheme:

1. Initializing the system at time t by choosing all particles' positions and velocities as well as a value for the time step Δt .
2. Computing the net force on each particle.
3. Integrating Newton's equations to find the particles' positions and velocities at the next step, i.e., time $t + \Delta t$.
4. Going back to step 2.

In MD² simulations physical quantities are calculated from time averages along the trajectories. Let $A(t) = A(\mathbf{r}_1(t), \dots, \mathbf{r}_N(t); \mathbf{v}_1(t), \dots, \mathbf{v}_N(t))$ be a dynamical quantity depending on positions and velocities. Its mean value is defined as

$$\overline{A(t)} = \frac{1}{N} \sum_{n=0}^{N-1} A(t_0 + n\Delta t), \quad (3.3)$$

where t_0 is an initial time. Physical quantities are conveniently characterized by a single relaxation time defined as the minimum time to reach equilibrium. If one is interested in equilibrium quantities, they should take averages starting from a given time $t_0 \gg \tau_A$. For systems that obey the ergodic hypothesis³, the evolution of a single MD simulation may be used to determine the macroscopic thermodynamic properties of all similar systems.

Based on how the differential equation 3.1 is discretized, one can find a different integration algorithm. One such algorithm is the Velocity-Verlet algorithm, which calculates new positions $\mathbf{r}_i(t + \Delta t)$ according to the following recipe [63]:

$$\mathbf{r}_i(t + \Delta t) = \mathbf{r}_i(t) + \mathbf{v}_i(t)\Delta t + \frac{\mathbf{F}_i(t)}{2m}\Delta t^2 \quad (3.4)$$

which is a Taylor series expansion. The new *on-site* velocities $\mathbf{v}_i(t + \Delta t)$ are then calculated as

$$\mathbf{v}_i(t + \Delta t) = \mathbf{v}_i(t) + \frac{\mathbf{F}_i(t) + \mathbf{F}_i(t + \Delta t)}{2m}\Delta t, \quad (3.5)$$

²MD stands for Molecular Dynamics.

³In physics and thermodynamics, the ergodic hypothesis means that all accessible microstates are equiprobable over a long time.

where $\mathbf{F}_i(t + \Delta t)$ is the future force which first needs to be calculated from the future positions in Equation 3.4. Although it may not be clear from Equations 3.4 and 3.5, it could be shown that in the Velocity-Verlet algorithm, the positions are calculated accurately up to the fourth-order in time [64]. This method is popular because of its simplicity, efficiency, stability properties, and time reversibility⁴. Note that time reversibility means that Equation 3.4 must remain invariant under the change of $\Delta t \rightarrow -\Delta t$. It should also be noted that the discrete-time velocity variables $\mathbf{v}_i(t)$ are fundamentally inconsistent with the discrete-time positions $\mathbf{r}_i(t)$, namely the discrete-time velocities are not precisely the conjugated variables of the simulated trajectory [65, 66].

Another essential feature of the Velocity Verlet algorithm is that it is a symplectic integrator. Symplectic integration algorithms have the property that their trajectories do conserve exactly a pseudo-energy, which differs from the actual energy by a small amount (vanishing as $\Delta t \rightarrow 0$). This avoids long-time drifts of the trajectories from the true ones owing to the accumulation of numerical errors during the time evolution. The Velocity-Explicit Verlet (VV) algorithm allows then for a constant-energy simulation, whereas we are looking for a numerical algorithm suited for a constant-temperature simulation. A variety of methods for conducting Molecular Dynamics simulations in the canonical ensemble have been proposed over the years. A very appealing class of such methods includes integrators for Langevin dynamics simulations, which we study in the following paragraphs.

To control the temperature in a Molecular Dynamics simulation, a Langevin thermostat can be used [67, 68]. In a closed NVT system, which is thermally coupled to a Langevin thermostat, Hamilton's equations of motion for the i th particle relative to an arbitrary fixed-space reference frame is written as

$$m_i \dot{\mathbf{r}}_i(t) = \dot{\mathbf{p}}_i(t) \quad \text{for } i = 1, 2, \dots, N, \quad (3.6)$$

$$\dot{\mathbf{p}}_i(t) = -\nabla_i U_N(\mathbf{r}_1(t), \dots, \mathbf{r}_i(t), \dots, \mathbf{r}_N(t)) + \mathbf{g}_i(t) \quad \text{for } i = 1, 2, \dots, N, \quad (3.7)$$

⁴time reversibility implies attractive conservation properties for the system's trajectory in the phase space for closed systems.

where U_N is the total particle interaction potential, ∇ is the gradient operator such that $-\nabla_i U_N$ is the net force calculated from the particle interaction potentials on the i th particle, and $\mathbf{g}_i(t)$ is a fictitious correction force which modifies the dynamics of the system. Since the total energy is conserved in Hamiltonian dynamics, $\mathbf{g}_i(t)$ becomes responsible for the variations that lead to the system thermalization. In standard Langevin dynamics, the correction force for a system in thermal equilibrium with its surrounding medium, i.e., the heat bath, is given by

$$\mathbf{g}_i(t)dt = -\gamma\mathbf{p}_i(t)dt + \sqrt{2m_i\gamma k_B T}dW_i(t) \quad \text{for } i = 1, 2, \dots, N, \quad (3.8)$$

where T is the absolute temperature of the thermal bath, $\gamma \geq 0$ is the collision rate or precisely, the Langevin thermal coupling constant between the system and the Langevin thermostat, and dW_i is a vector of independent Wiener noises⁵, normalized as

$$\langle dW_i(t)dW_j(t-t') \rangle = \delta(t')\delta_{ij}dt \quad \text{for } i, j = 1, 2, \dots, N \quad (3.9)$$

with $\delta(t')$ and δ_{ij} being the Dirac delta distribution and the Kronecker delta, respectively. The friction coefficient, i.e., $\Gamma \equiv m\gamma$, is related to the viscosity of the fluid through the viscous drag force formula in macroscopic hydrostatics:

$$m\gamma = 6\pi\eta d, \quad (3.10)$$

where η is the viscosity, and d is the effective diameter of the particle, assumed spherical. Thus, the first term on the right side of Equation 3.8 is a fictitious viscous-like force. The second term is a fluctuating force representing the incessant impacts of the molecules of a fictitious solvent on the particles.

The thermalization speed of a closed system coupled to a Langevin thermostat can be quantified by calculating the temporal evolution of the total kinetic energy, $K(t)$, of the system from Equations 3.7 and 3.8. By employing the Itô's lemma chain rule [69] along with Equation 3.9, the following expression is attained [70]:

$$dK(t) = -\frac{K(t) - \langle K \rangle}{\tau_k}dt + 2\sqrt{\frac{K(t)\langle K \rangle}{N\tau_k}}dW(t), \quad (3.11)$$

⁵A Wiener process is a zero-mean Gaussian random process. Thus, Wiener noise is the Gaussian white noise.

where $\tau_k \equiv (2\gamma)^{-1}$ is the relaxation time for the total kinetic energy, $K(t)$, and $\langle K \rangle = Nk_B T/2$ is the system's mean kinetic energy. Note that $dW(t)$ in Equation 3.11 is just a single noise term.

The difficulty in developing accurate numerical methods for Langevin dynamics stems from the non-analytic nature of the Wiener noise term, which also invalidates the technique of Taylor expansion used for the derivation of the Verlet schemes. Algorithms which solve the Langevin equation can only be exact in the limit of $\Delta t \rightarrow 0$ because of the presence of position-dependent forces. In the following subsection, we review a newly-developed kind of stochastic Verlet-type integration schemes, which was proven to provide a correct statistical measure for both the configurational and kinetic sampling in discrete-time Langevin systems. It was also demonstrated that the new algorithm is capable of providing exact thermodynamic responses for constant and harmonic potentials for any time step size within the Verlet stability criteria [71]. This numerical algorithm, which is called GJF, was first derived by N. Grønbech-Jensen and O. Farago in 2013 [66]. Five years later, a new numerical method based on the GJF method called GJF-2GJ was introduced by L. F. Grønbech Jensen and N. Grønbech-Jensen, which has turned out to be quite accurate, especially when it comes to the kinetic sampling of the phase space [71].

3.1.1 A Brief Review of the GJF and GJF-2GJ Methods

The GJF method was first derived in the well-known Velocity Verlet form. Then, it re-expressed in other popular forms such as the Störmer-Verlet, and Leap-Frog form [72]. The discrete-time, finite-difference GJF equations that address the Langevin equation in the Velocity-Explicit Verlet form are given by

$$\mathbf{r}_i(t + \Delta t) = \mathbf{r}_i(t) + b[\mathbf{v}_i(t)\Delta t + \frac{\mathbf{F}_i(t)}{2m}\Delta t^2 + \frac{\Delta t}{2m}dW_i(t)] \quad (3.12)$$

$$\mathbf{v}_i(t + \Delta t) = a\mathbf{v}_i(t) + \frac{a\mathbf{F}_i(t) + \mathbf{F}_i(t + \Delta t)}{2m}\Delta t + \frac{b}{m}dW_i(t), \quad (3.13)$$

where, to ensure the method is semi-symplectic⁶,

$$a = \frac{1 - \frac{\gamma\Delta t}{2}}{1 + \frac{\gamma\Delta t}{2}} \quad (3.14)$$

and

$$b = \frac{1}{1 + \frac{\gamma\Delta t}{2}} \quad (3.15)$$

with including the linear collision rate γ in Langevin dynamics. These equations can be written in other forms as well. For instance, the *on-site* position in the Störmer-Verlet GJF form is given by

$$\mathbf{r}_i(t + \Delta t) = 2b\mathbf{r}_i(t) - a\mathbf{r}_i(t - \Delta t) + \frac{b\Delta t^2}{m}\mathbf{F}_i(t) + \frac{b\Delta t}{2m}[dW_i(t - \Delta t) + dW_i(t)] \quad (3.16)$$

with the associated *on-site* velocity

$$\mathbf{v}_i(t) = \frac{\mathbf{r}_i(t + \Delta t) - (b - a)\mathbf{r}_i(t) - a\mathbf{r}_i(t - \Delta t)}{2b\Delta t} + \frac{1}{4m}[dW_i(t - \Delta t) - dW_i(t)], \quad (3.17)$$

where a and b are the same as in the Velocity-Verlet (VV) GJF method discussed earlier.

The GJF-2GJ method comes with some flexibility in how it can be expressed. This method combines the Velocity-Explicit Verlet (VV) and Leap-Frog (LF) GJF forms into a single form. We can take the starting point by introducing the *half-step* velocity as [71]

$$\mathbf{u}_i(t + \frac{\Delta t}{2}) = \frac{\mathbf{r}_i(t + \Delta t) - \mathbf{r}_i(t)}{\sqrt{b}\Delta t} = \sqrt{b}[\mathbf{v}_i(t) + \frac{\mathbf{F}_i(t)}{2m}\Delta t + \frac{dW_i(t)}{2m}], \quad (3.18)$$

where *on-site* \mathbf{r}_i and \mathbf{v}_i are given by Equations 3.12 and 3.13. Equation 3.18 is the definition of the GJF-2GJ method. One may express this method in different convenient ways. However, the result is always the same. It has been shown that the combination of the 2GJ *half-step* velocity with the GJF trajectory yields very robust statistical results for both kinetic and configurational properties for any time step size Δt within the stability range, even for highly nonlinear systems [73].

⁶A semi-symplectic integrator conserves a pseudo-Hamiltonian, instead of the system's Hamiltonian.

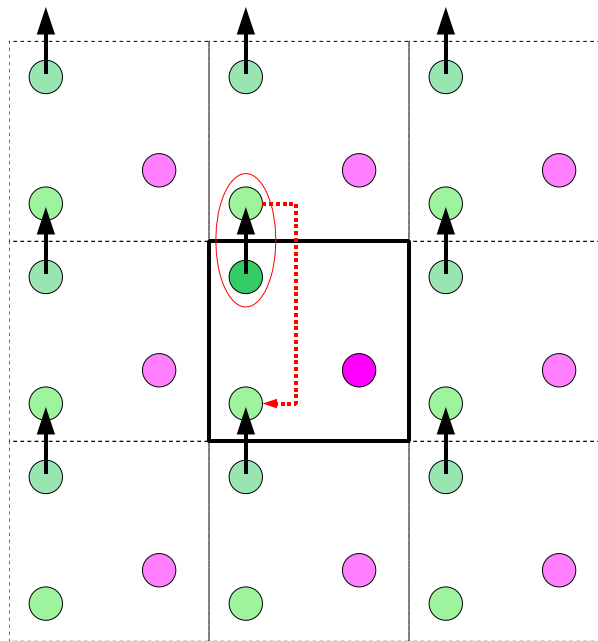


Figure 3.2: Schematic presentation of periodic boundary conditions (PBCs) in 2D. The original simulation box in the middle has eight images around it. From Wikipedia Commons, public domain, URL: https://en.wikipedia.org/w/index.php?title=Periodic_boundary_conditions&oldid=988336659

3.1.2 Periodic Boundary Conditions

In Molecular Dynamics simulations, the new position of a particle can be outside the range of the simulated box⁷. In such a case, one may introduce rigid walls for the simulation box so that the particle bounces back to the box, but then the simulation results will be influenced by these boundaries. To handle such a situation, the periodic boundary conditions, also known as cyclic boundary conditions, will be implemented. The cyclic boundary conditions treat the opposing boundary regions in every direction as if they are physically connected. Hence, if, for example, a particle passes through one side of the simulation box, it then reappears on the other side with the same velocity (see Figure 3.2 for a 2D simulation in the minimum-image convention⁸).

⁷A MD simulation box is often a parallelepiped of shape and size determined by the three vectors \mathbf{a} , \mathbf{b} , and \mathbf{c} which need not be equal in magnitude nor mutually orthogonal.

⁸The minimum-image convention is the most common form of the PBCs. In this approximation, particles only interact with the closest image of other particles.

3.1.3 Initialization

A Molecular Dynamics simulation begins with giving a set of initial positions and velocities to the particles, i.e. $(\mathbf{r}_1(0), \dots, \mathbf{r}_N(0); \mathbf{v}_1(0), \dots, \mathbf{v}_N(0))$. The positions can be initialized by creating particles on a lattice or randomly throughout the simulation box. The velocities can be selected from some distribution. For example, every velocity could be taken from a uniform distribution from a minimum to some maximum value, scaled to produce the desired temperature. Alternatively, it could be taken from a zero-mean Gaussian distribution with a sigma scaled to produce the requested temperature. One may impose the total linear momentum conservation condition to the simulation. So, if the initial selection yields

$$\mathbf{P}_{tot}(0) = \sum_{i=1}^N m_i \mathbf{v}_i(0) \neq 0, \quad (3.19)$$

we need to subtract from all velocities a value:

$$\mathbf{v}_i(0) \rightarrow \mathbf{v}_i(0) - \frac{\mathbf{P}_{tot}(0)}{Nm_i}. \quad (3.20)$$

to make the total linear momentum conserved. In the absence of external forces, it will remain constant at all times $t > 0$.

In Langevin dynamics, the random forces on different particles are completely independent. Thus, they do not necessarily sum to zero at each instant t , which may cause the central mass of the system to start wandering around over time. As a consequence, the total linear momentum is not conserved. For such a case, to impose the momentum conservation condition at all times $t > 0$, we must eliminate the CM⁹ displacement caused by the Langevin thermostat. In order to do so, the total random force is set precisely to zero by subtracting off an equal part of it from each particle in the system. Hence, the center-of-mass of a system with zero initial momentum will no longer drift over time.

Under periodic boundary conditions, the system's total linear momentum can be conserved, but not its total angular momentum. The conventional explanation of this situation is based on

⁹CM stands for Center of Mass

Noether's theorem [74], which states that the conservation of an isolated system's total angular momentum results from the rotational invariance of the Lagrangian \mathcal{L} . It is often emphasized (without providing any rigorous proof) that the absence of conservation of angular momentum in many-body systems under periodic boundary conditions is caused by breaking the rotational symmetries in the system [75]. Nonetheless, this approach fails to explain the simplest possible example: a periodic cell containing a single atom, whose Lagrangian is rotationally symmetric. For a detailed explanation of the situation, the interested reader is referred to [76].

3.1.4 Finite-Size Effects

Beyond the usual random statistical errors associated with averaging over a limited sample of particles in a computer simulation, systematic errors may also arise due to the finite size of the model system. In the conventional canonical MD simulations, two general types of finite-size effects are usually present [77, 78]:

1) Explicit (or ensemble) finite-size effects, caused by the suppression of density fluctuations upon fixing the number of particles in the canonical ensemble. In particular, the explicit finite-size effects alter the long-range tail of the total correlation function $h \equiv g - 1$ for an N -particle system. Suppose, for example, that $h(r)$ has power-law asymptotic behaviour [79] of the form $h(r) \rightarrow 1/r^n$ as $r \rightarrow \infty$ in an open system. Then, it will have the following asymptotic form in a closed NVT system due to the explicit finite-size effects:

$$\lim_{r \rightarrow \infty} h(r; N) \rightarrow \frac{1}{r^n} + \mathcal{O}\left(\left(\frac{1}{N}\right)^{n/d}\right) \rightarrow \mathcal{O}\left(\left(\frac{1}{N}\right)^{n/d}\right) \neq 0, \quad (3.21)$$

where d is the dimension of the system, and $\mathcal{O}((1/N)^{n/d})$ is the correction term of the order of $(1/N)^{n/d}$ added to account for the effect of the canonical ensemble. For example, for long-range dispersion forces ($n = 6$) in a finite 3D space ($d = 3$), we will have

$$\lim_{r \rightarrow \infty} h(r; N) \rightarrow \frac{1}{r^6} + \mathcal{O}\left(\left(\frac{1}{N}\right)^2\right). \quad (3.22)$$

2) Implicit (or anomalous) finite-size effects, resulting from considering specific boundary conditions for the simulated system (e.g., periodic boundary conditions give rise to an infinite set

of periodically replicating system cells so that correlations between adjacent cells can be significant). This kind of finite-size effect introduces anisotropy in the pair correlation functions, as reflected in the angular dependence of them. Hence, in a closed system with periodic boundary condition, the total correlation function is angular dependent, i.e.,

$$h(r) \rightarrow h(r, \theta, \phi). \quad (3.23)$$

In a finite system, both first- and second-order transitions also get smeared and shifted because of the explicit finite-size effects. Arguably, a distinguished first-order phase transition can only happen either in the thermodynamic limit or in an open system. If the transition is, for example, driven by the temperature T and occurs at a particular temperature $T_p(\infty)$ in the infinite system, then in a finite system, the transition may be smeared over a temperature region, where [80]

$$\Delta T_{\text{smeared}} \propto N^{-\theta/d}, \quad (3.24)$$

where θ is called rounding exponent, and d is the space dimensionality. This temperature region smoothly shrinks to zero as $N \rightarrow \infty$. For a more thorough discussion, the interested reader is referred to [80]. The finite-size effects vanish in the thermodynamic limit (or, macroscopic limit), which is defined as the limit of a system with $V \rightarrow \infty$, $N \rightarrow \infty$, $\rho = N/V$ is finite and constant [81].

3.1.5 Inter-Particle Interaction Potentials

For a system of N interacting identical particles, the interaction potential energy of the system, $U_N(\mathbf{r}_1, \dots, \mathbf{r}_N)$, can conveniently be expanded as a sum of n -body potentials [82, 83]:

$$U_N(\mathbf{r}_1, \dots, \mathbf{r}_N) = \sum_{i < j}^N u_2(\mathbf{r}_i, \mathbf{r}_j) + \sum_{i < j < k}^N u_3(\mathbf{r}_i, \mathbf{r}_j, \mathbf{r}_k) + \dots + \sum_{i < j < k < \dots < s}^N u_n(\mathbf{r}_i, \mathbf{r}_j, \mathbf{r}_k, \dots, \mathbf{r}_s) + \dots, \quad (3.25)$$

where u_n is the n -body potential. It should be noted that this series expansion should converge rapidly in most systems since the pairwise additive approximation, i.e., truncation of the above

series after the first term, is valid for many measurable properties. For example, pairwise additivity reveals that the hydrophobic effect is, indeed, a local phenomenon, and the hydrophobic interaction could be represented by a semiempirical force field [84]. It should be noted that this approximation is essentially suitable for the study of local phenomena. Despite this limitation, pairwise potentials are still widely used to study the effects of all ranges; This is mainly because of its simplicity as well as an incomplete understanding of the role of many-body effects.

Lennard-Jones Systems

A widely studied system is the Lennard-Jones system, which is defined as the one characterized by the following total interaction potential energy:

$$U_N(\mathbf{r}_1, \dots, \mathbf{r}_N) = \frac{1}{2} \sum_i^N \sum_j^N u_2(r_{ij}), \quad (3.26)$$

where $r_{ij} = |\mathbf{r}_i - \mathbf{r}_j|$ is the radial distance between the CM of particles i and j , and

$$u_2(r_{ij}) \equiv V_{LJ} = 4\varepsilon \left[\left(\frac{\sigma}{r_{ij}} \right)^{12} - \left(\frac{\sigma}{r_{ij}} \right)^6 \right] \quad (3.27)$$

is the Lennard-Jones potential, where ε is the depth of the potential well (usually referred to as dispersion energy), and σ is the radius at which the LJ potential energy is zero (often referred to as the effective radius of atoms). The LJ potential has a repulsive short-range term $\propto r^{-12}$ and an attractive long-range term $\propto -r^{-6}$. The origin of the attractive force is quantum-mechanical and is owing to fluctuating induced-dipoles. The repulsive term describes the Pauli repulsion at short distances of the interacting particles owing to overlapping electron orbitals. The exponent 12 was chosen exclusively because of ease of computation and had no theoretical justification. The LJ potential approximates very well the interactions in the noble massive gases, such as Ar, whose interactions are dominated by van der Waals forces and electrons are in closed shells.

The Lennard-Jones potential exhibits a pole at $r \rightarrow 0$, i.e. the potential energy diverges to $V_{LJ} \rightarrow \infty$, which can cause instabilities in MD simulations, for example, in which the particles are created with random coordinates; This is because the randomly generated coordinates may

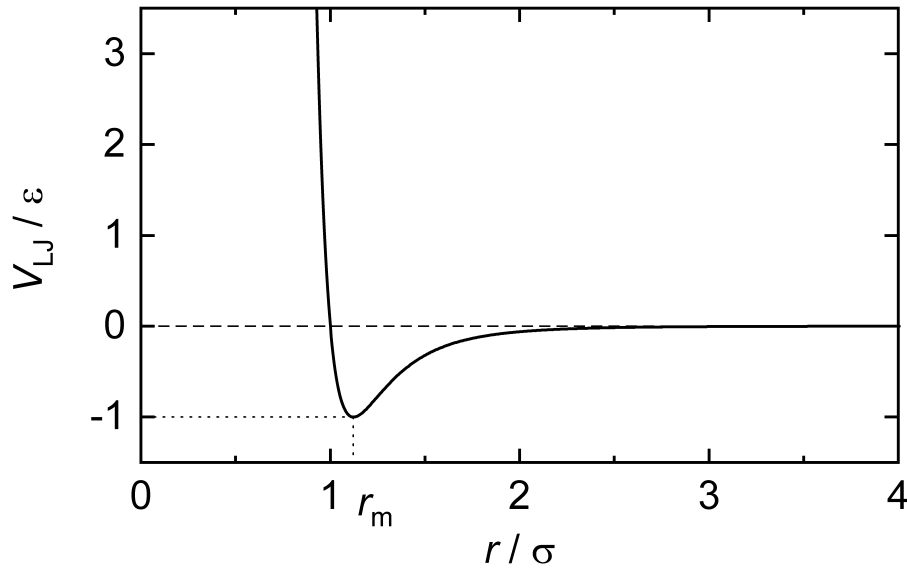


Figure 3.3: The reduced Lennard-Jones potential as a function of the reduced distance between a pair of particles. The potential minimum occurs at $r = r_m = 2^{1/6}\sigma$. From Wikipedia Commons, public domain, URL: https://en.wikipedia.org/w/index.php?title=Lennard-Jones_potential&oldid=989336384

overlap. On the contrary, the Lennard-Jones potential V_{LJ} converges to zero as $r \rightarrow \infty$, which may cause a serious problem from a numerical analysis standpoint. Infinitely-ranged potentials, such as the Lennard-Jones potential, are then truncated to a finite range $r \in (0, r_c]$, so that one may approximate the LJ potential with:

$$V_{LJ}^{ts}(r) = \begin{cases} V_{LJ}(r) - V_{LJ}(r_c), & \text{for } 0 < r \leq r_c \\ 0, & \text{for } r > r_c \end{cases}, \quad (3.28)$$

where $V_{LJ}^{ts}(r)$ is the truncated and shifted Lennard-Jones potential. The term $V_{LJ}(r_c)$ is usually a small constant shift and added to avoid jumps in the potential which would lead to an impulsive contribution to the pressure equal to [33]

$$\Delta P^{imp} = \frac{8\pi}{3}\rho^2 g(r_c)\epsilon\sigma^3 \left[\left(\frac{\sigma}{r_c}\right)^9 - \left(\frac{\sigma}{r_c}\right)^3 \right], \quad (3.29)$$

where $g(r_c) \approx 1$ is the radial distribution function at the radial cut-off distance r_c . Furthermore, the other advantage of using such a truncated and shifted potential is that the inter-atomic forces are always finite. Truncation of the inter-atomic interactions at r_c will, on the other hand, result

in a systematic shift in the coexistence lines. In particular, potential truncations and shifts have important consequences at low temperatures, especially in the vicinity of the triple point [85].

3.1.6 Reduced Units

In computer simulations, it is often convenient to express quantities such as temperature, density, and pressure in units other than the SI units¹⁰. As an example, expressing the quantities in reduced units allows us to benefit from the corresponding-states principle [86]. This law states that different states with different units can be compared to each other. However, this law only applies to systems consisting of one single particle type. In addition to the corresponding-states principle, there are two other important reasons for using reduced units:

- 1) In reduced units, since most numeric values are of the order of one, detecting errors is much easier now in computer simulations.
- 2) Moreover, using numbers of the order of one in computer algorithms minimizes the floating-point errors caused by the limited precision of processors [33].

Quantity	Reduced unit	Argon*
Time	$\sigma \sqrt{m/\varepsilon}$	2.1586 <i>ps</i>
Temperature	ε/k_B	119.55 <i>K</i>
Pressure	ε/σ^3	418.10×10^5 <i>Pa</i>
Mass Density	m/σ^3	1680.3 <i>Kg/m³</i>

Table 3.1: An example of the LJ reduced units for Argon. * The values for ε , σ , and m were retrieved from [87].

Dimensionless reduced units could be defined in a vast number of different ways. The most common one is based on the LJ potential parameters. For an LJ system, we can choose ε as the unit of energy, σ as the unit of length, and atomic mass m as the unit of mass, then express all other quantities in these basic units. See Table 3.1 for some examples.

¹⁰The International System of Units.

3.2 Simulation Details

In this thesis, our primary goal is to determine whether the initial structure's characteristics can affect the value of the system's relaxation time in a computer simulation. For this purpose, we have performed a number of Molecular Dynamics simulations using the LAMMPS¹¹ software package [88] and then measured the time-averaged RDF at thermal equilibrium for two different initial structural conditions, namely

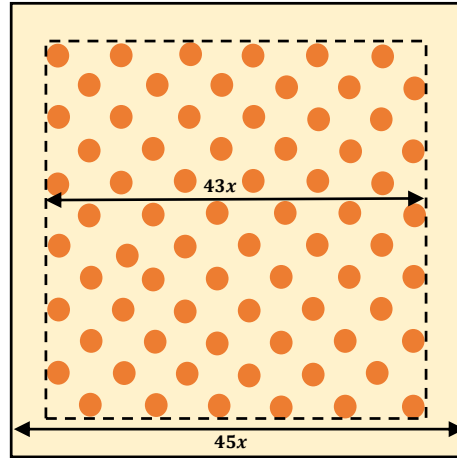
- 1) initial macroscopically inhomogeneous structure in the number density of atoms, and
- 2) initial macroscopically homogeneous structure in the number density of atoms.

All the quantities quoted here are in the LJ reduced units. A pure Lennard-Jones atomic fluid at a density of $\rho_0 = 0.0395$ was simulated in a Langevin $NVT\mathbf{P}$ ensemble, where \mathbf{P} is the system's total linear momentum, with periodic boundaries [89]. We have also truncated the LJ potential at $r_c = 2.5$ and shifted it up to make it continuous at the cut-off radius. The equations of motion were integrated using the GJF-2GJ algorithm with a timestep of $dt = 0.0007$ to ensure that the discretization errors are negligible [90].

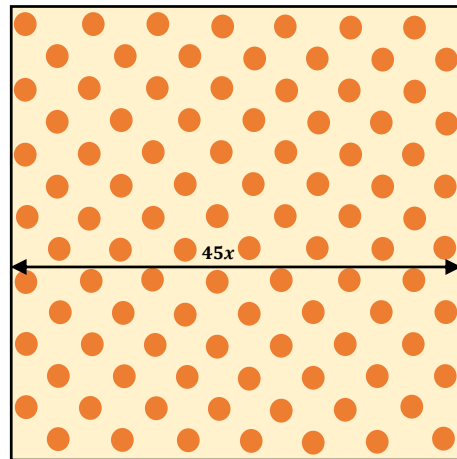
We first created 329252 particles at a temperature of $T = 0$ in the form of an FCC crystal, which consists of a total number of 43^3 cubic unit cells with a lattice constant of $x(\rho_0) = 4/\rho_0 = 4.661$. The resulting crystal is also located at the center of a cubic simulation box with a volume of $V = (45x)^3$. We used the series of commands shown in Table 3.2. Note that such a structure is macroscopically inhomogeneous in number density since there exist a considerable amount of empty spaces in the simulation box (see Figure 3.4a).

We then created 364500 particles at a temperature of $T = 0$ in the form of an FCC crystal, which consists of a total number of 45^3 cubic unit cells with a lattice constant of $x(\rho_0) = 4/\rho_0 = 4.661$ and fills the entire simulation box. We used the series of commands shown in Table 3.3. Note that such a structure is macroscopically uniform in number density (see Figure 3.4b).

¹¹LAMMPS is a classical Molecular Dynamics C++-based code aiming at material modelling. It is an acronym for Large-scale Atomic/Molecular Massively Parallel Simulator.



(a) Initial inhomogeneous structure



(b) Initial homogeneous structure

Figure 3.4: Initial crystalline structures (2D representation)

For both initial structures, the phase-space trajectories were first run for a duration of $\Delta t = t_e = 175$ in order to equilibrate the system thermally at a supercritical temperature of $T = 3.936$ for some multiples of a base Langevin thermal coupling constant $\gamma = \gamma_0 = 5/7$. As we will see in Chapter 4, $\Delta t = t_e = 175$ is more than enough time to equilibrate the system's temperature for all the γ values used. The trajectories were then run again for a duration of $\Delta t = t_{pro} = 525$ to calculate the mean RDF, $g(r)$, up to a maximum radius of $r_m = 25$. Finally, to ensure that the results are not limited only to the systems with crystalline initial structures, we have performed some extra MD simulations with amorphous initial structure (randomly-distributed particles),

Number	Command	Argument
1	lattice	fcc 0.0395
2	region	cube block 0 45 0 45 0 45
3	create_box	1 cube
4	region	sub block 1 44 1 44 1 44
5	create_atoms	1 region sub

Table 3.2: A series of commands in LAMMPS to create a macroscopically inhomogeneous crystalline structure in number density.

which fills the entire simulation box (see Figure 3.5). This is the only difference between the second and third batches of simulations. It should be stressed that this kind of initial structure is energetically unstable because randomly-generated particles are typically highly overlapped, and we already know $V_{LJ} \rightarrow \infty$ at $r \rightarrow 0$. Thus, it is necessary to locally minimize the system's potential energy U_N before running any normal dynamics. For this purpose, we performed a pre-energy minimization using the Conjugate Gradient algorithm for a duration of $\Delta t \simeq 2.1$. We used the series of commands shown in Table 3.4.

Number	Command	Argument
1	lattice	fcc 0.0395
2	region	cube block 0 45 0 45 0 45
3	create_box	1 cube
4	create_atoms	1 box

Table 3.3: A series of commands in LAMMPS to create a macroscopically homogeneous crystalline structure in number density.

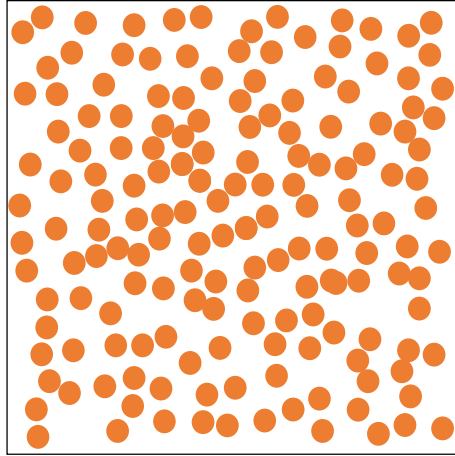


Figure 3.5: A stabilized amorphous structure (2D representation)

Number	Command	Argument
1	lattice	fcc 0.0395
2	region	cube block 0 45 0 45 0 45
3	create_box	1 cube
4	create_atoms	1 random 364500 564674 NULL
5	minimize	1.0E - 5 1.0E - 5 1000 100000

Table 3.4: A series of commands in LAMMPS to create a macroscopically homogeneous and stable amorphous structure in the number density of atoms.

3.2.1 Measuring the Mean RDF

To measure the mean RDF, i.e., $g(r)$, in a Molecular Dynamics simulation, a random particle should be selected (if all of the particles are equal). Then, the algorithm should look for other particles that have their center of mass within a distance r to $r + \delta r$ from the chosen particle. The algorithm does the same for a spherical shell extending from $r + \delta r$ to $r + 2\delta r$ and so forth for increasing radii of the spherical shell. The total number of particle pairs within a distance between r and $r + \delta r$ from a random particle i at time t is related to the instantaneous RDF, i.e.,

$g_i(r, t)$, as follows [91]:

$$g_i(r, t) = \lim_{\delta r \rightarrow 0} \frac{dn_i(r, t)}{4\pi(N_{pairs}/V)r^2\delta r}, \quad (3.30)$$

where r is the radial distance between a pair of particles, $dn_i(r, t)$ is the instantaneous number of particle pairs within a distance between r and $r + \delta r$ from the random particle i , V is the total volume of the simulation box, N_{pairs} the total number of particle pairs, and δr (≈ 0.0977 here) is the bin size. For calculating the mean RDF, we need to first take an average over all particles and then, use Equation 3.3 to compute its time average as

$$g(r) = \sum_{i=1}^N \overline{g_i(r, t)} = \frac{1}{N} \sum_{n=1}^N \sum_{i=1}^N g_i(r, t_e + n\Delta t), \quad (3.31)$$

where t_e is the equilibration time. So, we imply average over all times and particles within the simulation box by the word ‘‘mean’’ in the mean RDF. In the following chapter, we will present the results of our Molecular Dynamics simulations followed by some discussion regarding the results.

Chapter 4

Results and Discussion

In this chapter, we will first show that the system under both kinds of initial conditions (homogeneous and inhomogeneous) is in thermal equilibrium, i.e., the temperature is equilibrated, at all times $t > t_e$, where $t_e = 175$ is the equilibration time. Then, we present the results regarding the RDF measurements, followed by a section discussing and interpreting the results. Finally, we end this chapter with a short summary in Section 4.4.

4.1 Temperature Relaxation Time

4.1.1 Initial Inhomogeneous Crystalline Structure

In Figure 4.1, we have plotted the time evolution of the kinetic temperature¹ of the inhomogeneous crystalline structure shown in Figure 3.4a for several multiples of the Langevin coupling constant $\gamma_0 = 5/7$ to confirm that the system is in thermal equilibrium at all times $t > 175$. This figure shows that $t_e = \Delta t = 175$ is enough time for the system to come to thermal equilibrium with its surroundings, i.e., the thermal bath. Furthermore, it demonstrates that the stronger the thermal coupling between the system and the thermostat, the faster the system reaches thermal equilibrium. As mentioned earlier, in exponentially ergodic systems, the temporal evolution of

¹Kinetic temperature, T , is defined as the system's total kinetic energy per particle.

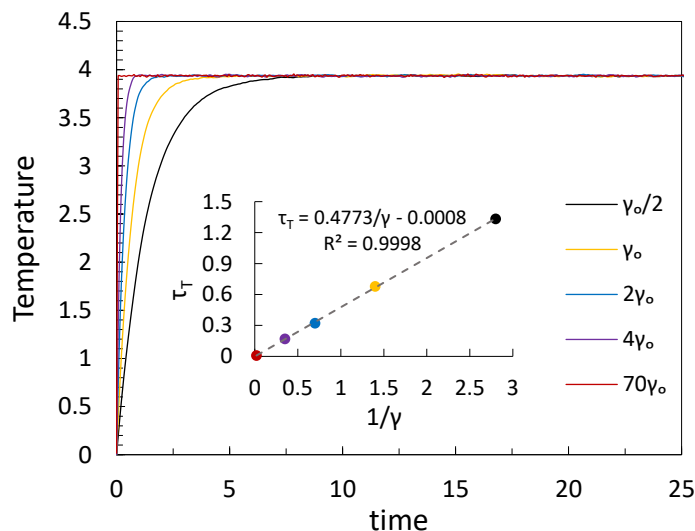


Figure 4.1: This figure illustrates the evolution of the kinetic temperature T with time during the equilibration phase for an initial inhomogeneous crystalline structure and some multiples of $\gamma = \gamma_0 = 5/7$. As it is evident, the higher the value of the Langevin coupling constant γ , the faster the system reaches thermal equilibrium. The inset depicts that the kinetic temperature relaxation time τ_T varies linearly with $1/\gamma$. To be precise, $\tau_T \simeq 1/2\gamma$. All the values are in the LJ reduced units.

quantities such as the temperature can be well approximated and fitted by an exponential function² [93]. The temperature relaxation time, which is denoted by τ_T , is then the time constant of the fitted exponential function. We have calculated the temperature relaxation time for each value of γ and plotted them versus $1/\gamma$ in the inset. As can be observed, the kinetic temperature relaxation time, τ_T , changes with the thermostat coupling constant γ via $\tau_T \simeq (2\gamma)^{-1}$, which is in agreement with what we expected from the theory (see Equation 3.11).

4.1.2 Initial Homogeneous Crystalline Structure

In Figure 4.2, similar to the inhomogeneous case, we have plotted the evolution of the kinetic temperature over time for the same values of the Langevin coupling constant, but for the initial homogeneous crystalline structure shown in Figure 3.4b. The graph also confirms that $t_e = 175$ is enough time for the system to reach thermal equilibrium with the surroundings. We have then

²The under-damped mean-field Langevin dynamics is exponentially ergodic [92].

calculated the temperature relaxation time τ_T for each value of γ and plotted them versus $1/\gamma$ in the inset. As can be seen, the kinetic temperature relaxation time, τ_T , varies with the Langevin coupling constant γ as $\tau_T(\gamma) \simeq 1/2\gamma$, which is again in agreement with the theory (see Equation 3.11). Comparing Figures 4.1 and 4.2, we realize the kinetic temperature relaxation time is, as expected, independent of the kind of initial structure used in a computer simulation.

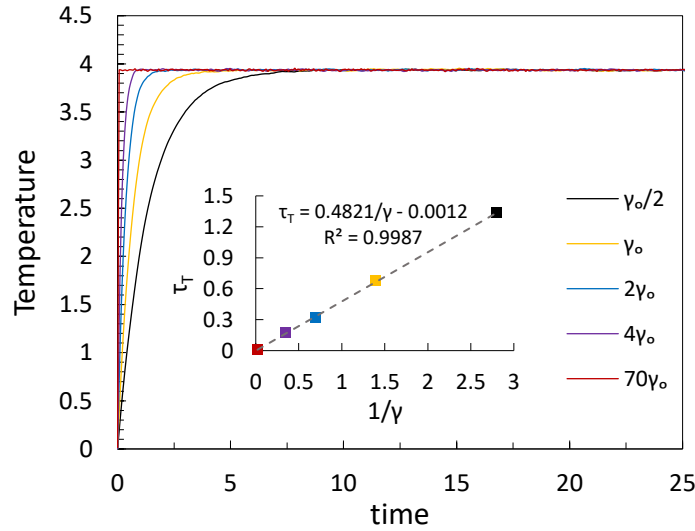


Figure 4.2: This figure illustrates the time evolution of the kinetic temperature T during the equilibration phase for an initial homogeneous crystalline structure and some multiples of $\gamma = \gamma_0 = 5/7$. As it is obvious, the higher the value of the Langevin coupling constant, the faster the system reaches thermal equilibrium. Besides, the inset shows that the kinetic temperature relaxation time, τ_T , varies with γ as $1/2\gamma$. All the values are in the LJ reduced units.

4.2 The Mean RDF

In this section, we have presented and plotted $r(g(r) - 1)$ instead of $g(r)$ for two main reasons:

1. We are interested only in examining the long-range deviation of $g(r)$ from for the ideal-gas RDF, i.e., $g^{id}(r) = 1$.
2. Also, because the deviation of $g(r)$ from one at large r can be negligible, we have scaled $g(r) - 1$ by r and plotted the scaled difference, i.e., $r(g(r) - 1)$.

4.2.1 Initial Inhomogeneous Crystalline Structure

In Figure 4.3, we have plotted the scaled total correlation function, $r(g(r)-1)$, for the case of the initial inhomogeneous crystalline structure of Figure 3.4a, the equilibration time $t_e = \Delta t = 175$, and several multiples of $\gamma = \gamma_0 = 5/7$. This figure shows clearly that the scaled total correlation function, as predicted in Equation 2.15, is not still relaxed to its final equilibrium value and, as a consequence, is γ -dependent at thermal equilibrium. In particular, for $r > 2.5$, $r(g(r)-1)$ varies linearly with a γ -dependent slope, which increases with γ , in the under-damped Langevin dynamics, i.e., weak thermal couplings, and non-linearly in the over-damped Langevin dynamics, i.e., strong thermal couplings. Such deviations from the expected behaviour could be possibly due to the two-body entropy s_2 is not being maximal yet. We can conclude that the condition of the equilibration of the kinetic temperature for the equilibration of the structure is necessary but not sufficient, especially when the system starts from an initial structure that is macroscopically inhomogeneous in the number density of atoms.

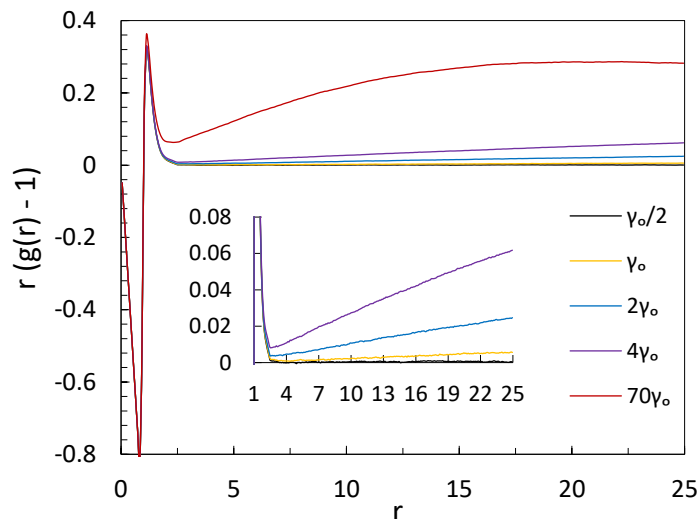


Figure 4.3: This figure illustrates $r(g(r) - 1)$ for the case of the inhomogeneous crystalline structure shown in Figure 3.4a, $t_e = 175$, and some multiples of the Langevin coupling constant $\gamma = \gamma_0 = 5/7$. This figure reveals that for an initial heterogeneous structure, the higher the value of the Langevin coupling constant, the more behaviour of the scaled total correlation function deviates from the expected one at thermal equilibrium, i.e., $r(g(r) - 1) = 0$ for $r > r_c (= 2.5)$. The inset shows a zoomed-in version of the figure. All the values are in the LJ reduced units.

4.2.2 Initial Homogeneous Structure

Crystalline Structure

In Figure 4.4, we have plotted the scaled total correlation function, i.e., $r(g(r) - 1)$, for the case of homogeneous crystalline structure of Figure 3.4b, the equilibration time $t_e = \Delta t = 175$, and several multiples of $\gamma = \gamma_0 = 5/7$. This figure reveals that the scaled total correlation function, unlike the inhomogeneous case, is completely independent of γ at thermal equilibrium. Hence, the RDF is well-equilibrated at thermal equilibrium for this case. This could be because, in this case, the structure is already homogeneous and, thus, does not need to expand to fill the entire simulation box and recover a homogeneous state. It is apparent that the system's equilibration process with an initial homogeneous structure usually takes less time compared to that with an initial inhomogeneous structure in the under-damped mean-field Langevin dynamics.

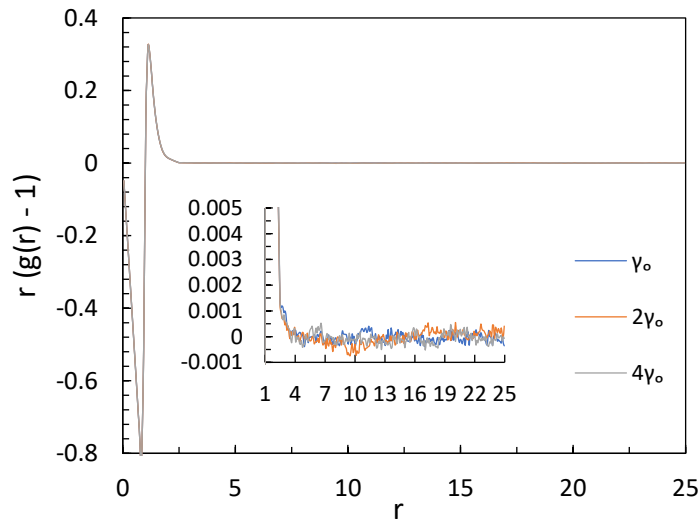


Figure 4.4: This figure presents $r(g(r) - 1)$ for the case of the homogeneous crystalline structure of Figure 3.4b, $t_e = 175$, and few multiples of the Langevin coupling constant $\gamma = \gamma_0 = 5/7$. This figure reveals that for an initial homogeneous structure, the scaled total correlation function is independent of γ at thermal equilibrium. The inset shows a zoomed-in version of the figure. All the values are in the LJ reduced units.

Amorphous Structure

We repeated the above computer experiment with an initial structure that was homogeneous and amorphous, as described at the end of Section 3.2 (see Figure 3.5 and Table 3.4). As expected, we found the same behaviour for the scaled total correlation function at thermal equilibrium as in the homogeneous crystalline case (see Figure 4.4). This suggests that no matter what pattern the particles originally formed from (random or orderly), as long as they are evenly distributed throughout the simulation box on average, we have

$$\tau_g \gtrsim \tau_T(\gamma) \quad (4.1)$$

in dilute systems, where τ_g is the long-time relaxation time for the RDF. From Equation 2.15, we know also that $\tau_g = \tau_{sys}$. Thus, for dilute systems with initial homogeneous structure in the under-damped mean-field Langevin dynamics,

$$\tau_{sys}^{hom} \gtrsim \tau_T(\gamma). \quad (4.2)$$

4.3 Discussion

In Figure 4.5, we have plotted the scaled total correlation function, $rh(r) = r(g(r) - 1)$, for the inhomogeneous case for $\gamma = 2\gamma_0 = 10/7$ and several multiples of $t_e = 175$. This figure reveals that the slope decreases with increasing the duration of the equilibration time t_e . Therefore, the non-zero slope is because the value of the equilibration time has not been enough to equilibrate the system's structure. In Figure 4.6, we have plotted the evolution of the slope of the scaled total correlation function for $r > r_c (= 2.5)$ with t_e for $\gamma = \gamma_0 = 5/7$ and $\gamma = 2\gamma_0 = 10/7$. This figure demonstrates that the slope in the under-damped mean-field Langevin dynamics varies with the equilibration time t_e in an exponential manner at thermal equilibrium for $r > r_c (= 2.5)$:

$$\text{The slope} \equiv \lim_{r \rightarrow \infty} h(r) = A(\gamma) \exp\{-t_e/\tau(\gamma)\}, \quad (4.3)$$

where $A(\gamma)$ was found to be some positive γ -dependent quantity for the initial inhomogeneous structure in Figure 3.4a. Equation 4.3 is simply the time average of Equation 2.15 for $r > 2.5$

during the production phase,

$$\begin{aligned} \lim_{r \rightarrow \infty} h(r) &\equiv \overline{\langle \lim_{r \rightarrow \infty} h(r, t) \rangle} = -\frac{1}{t_{pro}} \int_{t_e}^{t_e+t_{pro}} \frac{[\lim_{r \rightarrow \infty} \Delta u(r)]}{k_B T} \exp\{-t/\tau_{sys}\} dt \\ &= -\frac{[\lim_{r \rightarrow \infty} \Delta u(r)] \tau_{sys}}{t_{pro}} \exp\{-t_e/\tau_{sys}\} \end{aligned} \quad (4.4)$$

for $t_e + t_{pro} \gg \tau_{sys}$. Comparing Equations 4.3 and 4.4, it is obvious to see that $\tau(\gamma)$ is τ_{sys} and $A(\gamma)$ is $-[\lim_{r \rightarrow \infty} \Delta u(r)] \tau_{sys}(\gamma)/t_{pro}$, which implies that $\lim_{r \rightarrow \infty} \Delta u(r)$ for the inhomogeneous structure in Figure 3.4a is a negative constant, as we expected. The numerical results of $\tau(\gamma)$, obtained from Figure 4.6, i.e., $\tau(\gamma_0) = (0.013)^{-1}$ and $\tau(2\gamma_0) = (0.006)^{-1} \simeq 2\tau(\gamma_0)$, suggests an increasing behaviour for $\tau(\gamma)$ with increasing γ . Besides, by comparing these values with those values obtained from Figures 4.1 and 4.2 for $\tau_T(\gamma_0)$ and $\tau_T(2\gamma_0)$, we find that

$$\tau(\gamma) \gg \tau_T(\gamma) \quad (4.5)$$

for an initial inhomogeneous structure, which is an essential result of this thesis. Thus, we can conclude that for a dilute inhomogeneous system in contact with the Langevin thermostat:

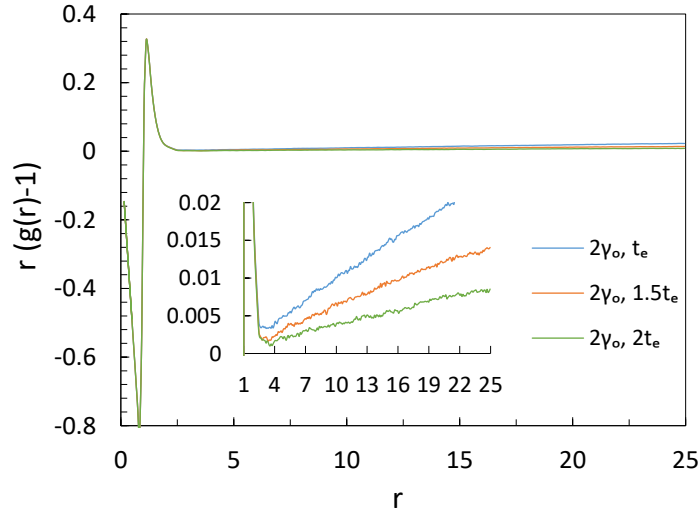


Figure 4.5: This figure presents $r(g(r) - 1)$ of the homogeneous crystalline structure of Figure 3.4b for the case of the Langevin coupling constant $\gamma = 2\gamma_0 = 10/7$ and few multiples of $t_e = 175$. This figure demonstrates that the slope of the scaled total correlation function, i.e., $g(r) - 1$, decreases continuously with increasing t_e . The inset shows a zoomed-in version of the figure. All the values are in the LJ reduced units.

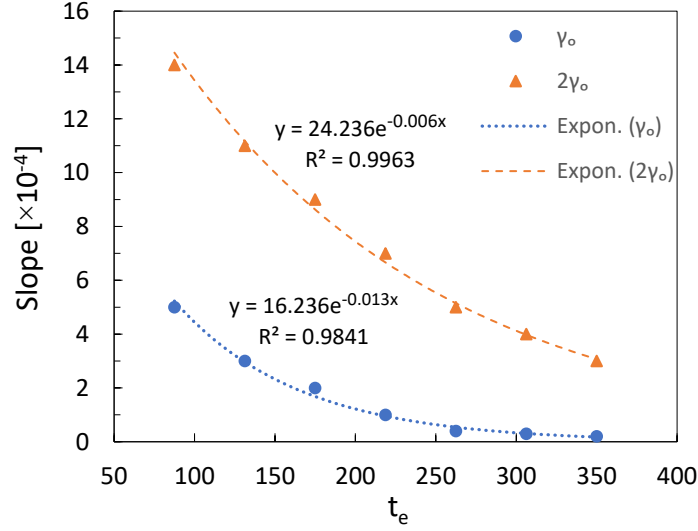


Figure 4.6: This figure illustrates how the slope of the scaled total correlation function for $r > r_c (= 2.5)$ changes with the equilibration time t_e . As it is evident, the slope decays exponentially with a γ -dependent time constant, which increases apparently with increasing γ . Based on Equation 2.15, this time constant is the system relaxation time. All the values are in the LJ reduced units.

- 1) $\uparrow \tau_{sys}^{inhom}(\gamma) \sim \gamma \uparrow$
- 2) $\tau_{sys}^{inhom}(\gamma) \gg \tau_T(\gamma)$

The first result is in contrast to what is found for the equilibration of the kinetic temperature in Section 4.1, where $\tau_T(\gamma) \simeq (2\gamma)^{-1}$ and $\downarrow \tau_T(\gamma) \sim \gamma \uparrow$.

4.4 Summary

In this section, we summarise the main results found in this thesis:

- 1) The long-time equilibration of the RDF for a dilute system in the under-damped mean-field Langevin dynamics can be written at each time t as follows:

$$\langle g(r, t; \gamma) \rangle = 1 - \frac{\Delta u(r)}{k_B T} \exp\{-t/\tau_{sys}(\gamma)\}, \quad (4.6)$$

where $\Delta u(r)$ is called residual potential and depends on the system's averaged configuration, T is the equilibrium temperature between the system and the thermal bath, and τ_{sys} is the system

relaxation time.

2) The system relaxation time, τ_{sys} , is much longer than the kinetic temperature relaxation time if the initial structure is macroscopically inhomogeneous in number density and in contact with the Langevin thermostat. In addition, $\tau_{sys}(\gamma)$ was found to be an increasing function of γ in the under-damped Langevin dynamics, which was quite predictable due to the disruptive influence of the stochastic force in the Langevin equation on structural relaxation times.

3) The system relaxation time, τ_{sys} , is almost γ -independent and of the order of the temperature relaxation time for dilute systems with initial homogeneous structure (random or orderly).

4) Comparing the system relaxation time for the both kinds of initial structures, we realize that

$$\tau_{sys}^{inhom} \gg \tau_{sys}^{hom}. \quad (4.7)$$

5) The kinetic temperature relaxation time, τ_T , is completely independent of the system's initial structure and decreases with increasing γ , i.e.,

$$\downarrow \tau_T(\gamma) \sim \gamma \uparrow. \quad (4.8)$$

Chapter 5

Conclusion

We found out that the system's structural relaxation time is not completely independent of the initial structure in a Molecular Dynamics simulation. In particular, we showed that if the initial structure is macroscopically inhomogeneous in the number density ρ , it takes more time for the system's structure to equilibrate fully. We also found out a not-well-equilibrated structure in the under-damped Langevin dynamics manifests itself by an almost uniform shift in the RDF for $r \gg r_c$, where r_c is the cut-off radius. To avoid such an artifact, we recommend using either a small value for the coupling constant γ or other commands to create the initial structure such as “**create_atoms** box” in LAMMPS, which fills the entire simulation box with particles and treats the system's periodic boundaries carefully, or “**create_atoms** random NULL”, which creates particles at random positions all over the simulation box.

The other important message of this thesis is that the system relaxation time is not always of the order of the kinetic temperature relaxation time. So, thermal equilibrium does not mean thermodynamic equilibrium. The structural relaxation time should also be taken into account. To check if the structure is in equilibrium (thermally and structurally), we recommend plotting $\ln r(g(r) - 1)$. If it exhibits a pure logarithmic behaviour for $r \gg \xi$, where ξ is the correlation length, it means that the structure has not reached equilibrium yet. Note that in thermodynamic equilibrium, $\ln r(g(r) - 1)$ for $r \gg \xi$ exhibits a fluctuating behaviour owing to the presence of

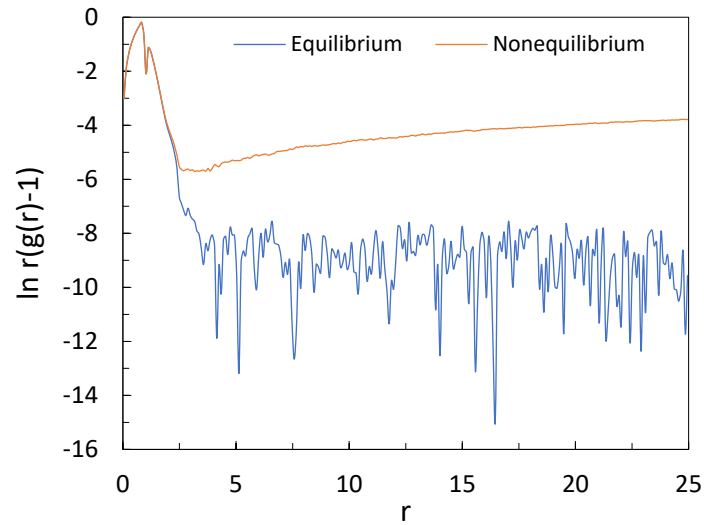


Figure 5.1: This figure compares the equilibrium and non-equilibrium $\ln r(g(r) - 1)$ for a system which has had an initial inhomogeneous structure in the number density. As $\ln(x)$ of a negative x is not mathematically defined, we plotted $\ln r|g(r) - 1|$. All the values are in the LJ reduced units.

statistical errors around the numerical accuracy of the algorithm. In Figure 5.1, we have plotted $\ln r(g(r) - 1)$ for both equilibrium and non-equilibrium systems which have started from initial inhomogeneous structures in the number density ρ .

Bibliography

- [1] C. Kittel and H. Kroemer. *Thermal Physics*. W. H. Freeman and Company, 2nd edition, March 1980.
- [2] Z. Yan. General thermal wavelength and its applications. *European Journal of Physics*, 21(6):625–631, November 2000.
- [3] J. Yvon and Y. Rocard. *La theorie statistique des fluides et l'equation d'etat*. Paris: Hermann & Cie, 1935.
- [4] N. N. Bogoliubov. Kinetic Equations (in English). *Journal of Physics-USSR*, 10(3):256–274, 1946.
- [5] J. G. Kirkwood. The statistical mechanical theory of transport processes I. general theory. *The Journal of Chemical Physics*, 14(3):180–201, March 1946.
- [6] M. Born and H. S. Green. A general kinetic theory of liquids I. the molecular distribution functions. *Proceedings of the Royal Society of London. Series A. Mathematical and Physical Sciences*, 188(1012):10–18, December 1946.
- [7] J. P. Hansen and I. R. McDonald. *Theory of Simple Liquids: With Applications to Soft Matter*. Academic Press, 4th edition, October 2013.
- [8] C. G. Gray and K. E. Gubbins. *Theory of Molecular Fluids: Fundamentals*, volume 1. Oxford University Press, New York, 1984.

- [9] J. M. Haile and C. G. Gray. Spherical harmonic expansions of the angular pair correlation function in molecular fluids. *Chemical Physics Letters*, 76(3):583–588, December 1980.
- [10] S. V. Savenko and M. Dijkstra. Asymptotic decay of the pair correlation function in molecular fluids: Application to hard rods. *Physical Review E*, 72(2):021202, August 2005.
- [11] M. E. Rose. *Elementary Theory of Angular Momentum*. New York: Wiley, 1957.
- [12] G. E. O. Giacaglia. Hansen coefficients and generalized spherical harmonics. *Publications of the Astronomical Society of Japan*, 39(1):171–178, January 1987.
- [13] R. E. Dinnebier and S. J. L. Billinge, editors. *Powder Diffraction: Theory and Practice*. The Royal Society of Chemistry, 1st edition, March 2008.
- [14] J.L. Barrat and J.P. Hansen. *Basic Concepts for Simple and Complex Liquids*. Cambridge University Press, New York, March 2003.
- [15] K. Zhang. On the concept of static structure factor. *arXiv:1606.03610*, June 2016.
- [16] R. J.F. Leote De Carvalho, R. Evans, D. C. Hoyle, and J. R. Henderson. The decay of the pair correlation function in simple fluids: Long- versus short-ranged potentials. *Journal of Physics: Condensed Matter*, 6(44):9275–9294, October 1994.
- [17] K. E. Newman. Kirkwood–buff solution theory: derivation and applications. *Chemistry Society Reviews*, 23(1):31–40, 1994.
- [18] D. Chandler. *Introduction to Modern Statistical Mechanics*. Oxford University Press, USA, September 1987.
- [19] J. R. Henderson. Wetting phenomena and the decay of correlations at fluid interfaces. *Physical Review E*, 50(6):4836–4846, December 1994.

- [20] J. Chai, S. Liu, and X. Yang. Molecular dynamics simulation of wetting on modified amorphous silica surface. *Applied Surface Science*, 255(22):9078–9084, August 2009.
- [21] M. Dijkstra and R. Evans. A simulation study of the decay of the pair correlation function in simple fluids. *Journal of Chemical Physics*, 112(3):1449–1456, January 2000.
- [22] R. Evans and J. R. Henderson. Pair correlation function decay in models of simple fluids that contain dispersion interactions. *Journal of Physics: Condensed Matter*, 21(47):474220, November 2009.
- [23] D. Stopper, H. Hansen-Goos, R. Roth, and R. Evans. On the decay of the pair correlation function and the line of vanishing excess isothermal compressibility in simple fluids. *Journal of Chemical Physics*, 151(1):014501, July 2019.
- [24] C. Vega, L. F. Rull, and S. Lago. Location of the fisher-widom line for systems interacting through short-ranged potentials. *Physical Review E*, 51(4):3146–3155, April 1995.
- [25] A. G. Vorontsov and D. A. Kuts. Structural changes of simple expanded liquids at high temperatures. *Journal of Physics: Conference Series*, 98(1):012004, February 2008.
- [26] J.R. Henderson and Z.A. Sabeur. Instability of the liquid state at high density: a detailed numerical analysis. *Molecular Physics*, 82(4):765–779, February 1994.
- [27] J. G. Kirkwood and E. Monroe. Statistical Mechanics of Fusion. *The Journal of Chemical Physics*, 9(7):514–526, 1941.
- [28] R. Eisenschitz and F. London. Über das verhältnis der van der waalsschen kräfte zu den homöopolaren bindungskräften. *Zeitschrift für Physik*, 60:491–527, July 1930.
- [29] F. London. The General Theory Of Molecular Forces. *Transactions of the Faraday Society*, 33:8–26, January 1937.

- [30] M. Li, J. R. Reimers, J. F. Dobson, and T. Gould. Faraday cage screening reveals intrinsic aspects of the van der waals attraction. *Proceedings of the National Academy of Sciences*, 115(44):E10295–E10302, October 2018.
- [31] M. P. Allen and D. J. Tildesley. *Computer Simulation of Liquids*. Oxford University Press, 2nd edition, July 2017.
- [32] G.A. Martynov. Structure of fluids from the statistical mechanics point of view. *Journal of Molecular Liquids*, 106(2):123–130, July 2003.
- [33] D. Frenkel and B. Smit. *Understanding Molecular Simulation: From Algorithms to Applications*. Academic Press, 2nd edition, November 2001.
- [34] D. H. Tsai. The virial theorem and stress calculation in molecular dynamics. *The Journal of Chemical Physics*, 70(3):1375–1382, February 1979.
- [35] J. Jeans. *The Dynamical Theory of Gases*. Cambridge University Press, 4th edition, July 2009.
- [36] R. Clausius, T. A. Hirst, and J. Tyndall. *The Mechanical Theory of Heat: With its Applications to the Steam-engine and to the Physical Properties of Bodies*. London: John Van Voorst, May 1867.
- [37] P. Županović and D. Kuić. Relation between Boltzmann and Gibbs entropy and example with multinomial distribution. *Journal of Physics Communications*, 2(4):045002, April 2018.
- [38] M. Plischke and B. Bergersen. *Equilibrium Statistical Physics*. World Scientific, 3rd edition, April 2006.
- [39] L.D. Landau and E.M. Lifshitz. *Statistical Physics, part 1*. Butterworth-Heinemann, 3rd edition, January 1980.

- [40] H.S. Green. *The Molecular Theory of Fluids*. North-Holland, Amsterdam, 1952.
- [41] J. G. Kirkwood and E. M. Boggs. The Radial Distribution Function in Liquids. *The Journal of Chemical Physics*, 10(6):394–402, 1942.
- [42] D. C. Wallace. On the role of density fluctuations in the entropy of a fluid. *The Journal of Chemical Physics*, 87(4):2282–2284, August 1987.
- [43] B. B. Laird and A. D.J. Haymet. Calculation of the entropy from multiparticle correlation functions. *Physical Review A*, 45(8):5680–5689, April 1992.
- [44] M. Widom and M. Gao. First principles calculation of the entropy of liquid aluminum. *Entropy*, 21(2):131, January 2019.
- [45] A. Baranyai and D. J. Evans. Direct entropy calculation from computer simulation of liquids. *Physical Review A*, 40(7):3817–3822, October 1989.
- [46] R. D. Mountain and H. J. Raveché. Entropy and Molecular Correlation Functions in Open Systems. II Two- and Three-Body Correlations. *The Journal of Chemical Physics*, 55(5):2250–2255, 1971.
- [47] A. Baranyai and D. J. Evans. Three-particle contribution to the configurational entropy of simple fluids. *Physical Review A*, 42(2):849–857, July 1990.
- [48] D. S. Lemons and A. Gythiel. Paul Langevin’s 1908 paper “On the Theory of Brownian Motion” [“Sur la théorie du mouvement brownien,” C. R. Acad. Sci. (Paris) 146, 530–533 (1908)]. *American Journal of Physics*, 65(11):1079, 1997.
- [49] E. Gibney. The quest to crystallize time. *Nature*, 543:164–166, March 2017.
- [50] J. C. Maxwell. IV. On the dynamical theory of gases. *Philosophical Transactions of the Royal Society of London*, 157:49–88, January 1867.
- [51] I. N. Levine. *Physical Chemistry*. McGraw-Hill Education, 6th edition, May 2008.

- [52] W. Greiner, L. Neise, H. Stocker, H. Stöcker, and D. Rischke. *Thermodynamics and Statistical Mechanics*. Classical Theoretical Physics. Springer, May 1995.
- [53] F. Reif. *Fundamentals of Statistical and Thermal Physics*. Waveland Press, January 2009.
- [54] R. L. Davidchack, R. Handel, and M. V. Tretyakov. Langevin thermostat for rigid body dynamics. *Journal of Chemical Physics*, 130(23):234101, June 2009.
- [55] J. J. Waterson and F. Beaufort. On the physics of media that are composed of free and perfectly elastic molecules in a state of motion. *Abstracts of the Papers Communicated to the Royal Society of London*, 5:604–604, January 1851.
- [56] L. Van Hove. Correlations in space and time and born approximation scattering in systems of interacting particles. *Physical Review*, 95(1):249–262, July 1954.
- [57] N. Metropolis. The Beginning of the Monte Carlo Method. *Los Alamos Science (Special Issue)*, 15:125–130, 1987.
- [58] K. A. Fichthorn and W. H. Weinberg. Theoretical foundations of dynamical Monte Carlo simulations. *The Journal of Chemical Physics*, 95(2):1090–1096, January 1991.
- [59] E. Paquet and H. L. Viktor. Molecular dynamics, Monte Carlo simulations, and Langevin dynamics: A computational review. *BioMed Research International*, February 2015.
- [60] B. J. Alder and T. E. Wainwright. Studies in Molecular Dynamics. I. General Method. *The Journal of Chemical Physics*, 31(2):459–466, August 1959.
- [61] G. G. Batrouni, G. R. Katz, A. S. Kronfeld, G. P. Lepage, B. Svetitsky, and K. G. Wilson. Langevin simulations of lattice field theories. *Physical Review D*, 32(10):2736–2747, November 1985.
- [62] R. Mannella. Numerical stochastic integration for quasi-symplectic flows. *SIAM Journal on Scientific Computing*, 27(6):2121–2139, 2006.

- [63] L. Verlet. Computer “Experiments” on Classical Fluids. I. Thermodynamical Properties of Lennard-Jones Molecules. *Physical Review*, 159(1):98–103, July 1967.
- [64] T. Pang. *An Introduction to Computational Physics*. Cambridge University Press, 2nd edition, January 2006.
- [65] R. W. Pastor, B. R. Brooks, and A. Szabo. An analysis of the accuracy of Langevin and molecular dynamics algorithms. *Molecular Physics*, 65(6):1409–1419, June 1988.
- [66] N. Grønbech-Jensen and O. Farago. A simple and effective Verlet-type algorithm for simulating Langevin dynamics. *Molecular Physics*, 111(8):983–991, February 2013.
- [67] T. Schneider and E. Stoll. Molecular-dynamics study of a three-dimensional one-component model for distortive phase transitions. *Physical Review B*, 17(3):1302–1322, February 1978.
- [68] A. Brünger, C. L. Brooks, and M. Karplus. Stochastic boundary conditions for molecular dynamics simulations of ST2 water. *Chemical Physics Letters*, 105(5):495–500, March 1984.
- [69] C. Gardiner. *Stochastic Methods: A Handbook for the Natural and Social Science*. Springer Series in Synergetics. Springer, 4th edition, January 2009.
- [70] G. Bussi and M. Parrinello. Stochastic thermostats: comparison of local and global schemes. *Computer Physics Communications*, 179(1):26–29, July 2008.
- [71] L. F. Grønbech Jensen and N. Grønbech-Jensen. Accurate Configurational and Kinetic Statistics in Discrete-Time Langevin Systems. *Molecular Physics*, 117(18):2511–2526, January 2019.
- [72] N. Grønbech-Jensen, N. R. Hayre, and O. Farago. Application of the G-JF discrete-time thermostat for fast and accurate molecular simulations. *Computer Physics Communications*, 185(2):524–527, February 2014.

- [73] N. Grønbech-Jensen. Complete Set of Stochastic Verlet-Type Thermostats for Correct Langevin Simulations. *Molecular Physics*, 118(8):e1662506, 2020.
- [74] E. Noether. Invariante variationsprobleme. *Nachrichten von der Gesellschaft der Wissenschaften zu Göttingen, Mathematisch-Physikalische Klasse*, 1918:235–257, 1918.
- [75] D. Frenkel. Simulations: The dark side. *European Physical Journal Plus*, 128(10), January 2013.
- [76] V.A. Kuzkin. On angular momentum balance for particle systems with periodic boundary conditions. *ZAMM - Journal of Applied Mathematics and Mechanics / Zeitschrift für Angewandte Mathematik und Mechanik*, 95(11):1290–1295, 2015.
- [77] J. L. Lebowitz and J. K. Percus. Thermodynamic Properties of Small Systems. *Physical Review*, 124(6):1673–1681, December 1961.
- [78] J. L. Lebowitz and J. K. Percus. Long-Range Correlations in a Closed System with Applications to Nonuniform Fluids. *Physical Review*, 122(6):1675–1691, June 1961.
- [79] J E Enderby, T Gaskell, and N H March. Asymptotic form of correlation functions in classical fluids and in liquid Helium 4. *Proceedings of the Physical Society*, 85(2):217–221, February 1965.
- [80] K. Binder. Finite size effects on phase transitions. *Ferroelectrics*, 73(1):43–67, March 1987.
- [81] K. Huang. *Statistical Mechanics*. Wiley, 2nd edition, May 1987.
- [82] M. J. Elrod and R. J. Saykally. Many-body effects in intermolecular forces. *Chemical Reviews*, 94(7):1975–1997, November 1994.
- [83] Erin E. Dahlke and Donald G. Truhlar. Assessment of the pairwise additive approximation and evaluation of many-body terms for water clusters. *Journal of Physical Chemistry B*, 110(22):10595–10601, May 2006.

- [84] J. Wu and J. M. Prausnitz. Pairwise-additive hydrophobic effect for alkanes in water. *Proceedings of the National Academy of Sciences of the United States of America*, 110(28):9512–9515, July 2008.
- [85] A. Ahmed and R. J. Sadus. Effect of potential truncations and shifts on the solid-liquid phase coexistence of Lennard-Jones fluids. *The Journal of Chemical Physics*, 133(12):124515, July 2010.
- [86] J.W. Tester and M. Modell. *Thermodynamics and Its Applications*. Prentice Hall, 3rd edition, August 1996.
- [87] M. T. Dove. *Structure and Dynamics: An Atomic View of Materials*. Oxford Master Series in Condensed Matter Physics. Oxford University Press, UK, May 2003.
- [88] S. Plimpton. Fast Parallel Algorithms for Short-Range Molecular Dynamics. *Journal of Computational Physics*, 117(1):1–19, March 1995.
- [89] J. A. White, F. L. Román, A. González, and S. Velasco. Periodic boundary conditions and the correct molecular-dynamics ensemble. *Physica A: Statistical Mechanics and its Applications*, 387(27):6705–6711, December 2008.
- [90] R. L. Davidchack. Discretization errors in molecular dynamics simulations with deterministic and stochastic thermostats. *Journal of Computational Physics*, 229(24):9323–9346, December 2010.
- [91] B. G. Levine, J. E. Stone, and A. Kohlmeyer. Fast Analysis of Molecular Dynamics Trajectories with Graphics Processing Units-Radial Distribution Function Histogramming. *Journal of Computational Physics*, 230(9):3556–3569, May 2011.
- [92] A. Kazeykina, Z. Ren, X. Tan, and J. Yang. Ergodicity of the underdamped mean-field Langevin dynamics. *arXiv:2007.14660*, July 2020.

- [93] J. E. Basconi and M. R. Shirts. Effects of temperature control algorithms on transport properties and kinetics in molecular dynamics simulations. *Journal of Chemical Theory and Computation*, 9(7):2887–2899, May 2013.

Curriculum Vitae

Name: Omid Mozafar

Post-Secondary Education and The University of Tehran

Degrees: Tehran, Tehran, Iran

2013 - 2018 BSc

The University of Western Ontario

London, Ontario, Canada

2018 - 2020 MSc

Honours and Awards: Western Graduate Research Scholarship

2018 - 2020

Graduate Teaching Assistant Award

London, ON

2018 - 2020

Related Work Experience: Teaching Assistant

The University of Western Ontario

2018 - 2020